Title	Electron Spin Echo of Minerals for Dating and Dosimetry
Author(s)	河野, 日出夫
Citation	大阪大学, 1997, 博士論文
Version Type	VoR
URL	https://doi.org/10.11501/3132584
rights	
Note	

Electron Spin Echo of Minerals for Dating and Dosimetry

by

Hideo KOHNO

DISSERTATION IN PHYSICS

1997

OSAKA UNIVERSITY

GRADUATE SCHOOL OF SCIENCE

TOYONAKA, OSAKA, JAPAN

Electron Spin Echo of Minerals for Dating and Dosimetry

by

Hideo KOHNO

DISSERTATION IN PHYSICS

OSAKA UNIVERSITY

GRADUATE SCHOOL OF SCIENCE

TOYONAKA, OSAKA

Abstract

Continuous wave (cw-) electron spin resonance (ESR) has been applied to radiation dosimetry and dating by detecting paramagnetic defects and radicals. One of the most serious problems in ESR dating and dosimetry is that the signal is interfered by other overlapping signals. One advantage of pulsed ESR method which enables the observation of the electron spin echo (ESE) is the selective detection of a particular signal from the overlapping signals. This technique has so far not been applied to the ESR dating and dosimetry. The aim of the present thesis is to study the ESE of defects in some minerals for dating purpose.

Experimental results on $CaCO_3$ (aragonite and calcite) are described in Chapter 2. The signal of the isotropic CO_2^- in gamma-irradiated aragonite can be almost removed in the field sweep ESE spectrum, and the selective detection of orthorhombic CO_2^- becomes possible. Intense signals of Mn^{2+} are also removed and the selective detection of the signal of SO_3^- is made for calcitic shell. The ESE intensity of CO_2^- in aragonitic shell is enhanced by the additive gamma-irradiation giving a paleodose.

In Chapter 3, E' centers in quartz (SiO_2) irradiated by alpha-rays (He^+-beam), neutrons, and those produced by gamma-irradiation after crushing as well as in gamma-irradiated silica glass are investigated. E' centers in crushed quartz are localized in amorphous region presumably around micro cracks. The phase relaxation times are compared with the line-widths and the ratios of homogeneous to inhomogeneous broadening.

In Chapter 4, results of ESE measurements of evaporites such as $NaHCO_3$ (nahcolite), $CaSO_4 \cdot 2H_2O$ (gypsum) and $BaSO_4$ (barite) are discussed. Selective detection of ESE of HCO_2 (CO_2^-) in gamma-irradiated nahcolite are made. A natural nahcolite sample is dated by ESE. ESE of SO_3^- is selectively detected in gamma-irradiated synthetic gypsum, while no echo is observed in He^+-irradiated sample. A new technique is proposed to estimate a paleodose using the dose-dependence of the phase relaxation time. There is a linear correlation between the cw-ESR intensity and the reciprocal of the phase relaxation time of a hole-type center in a natural barite measured at 77 K.

Lastly, a new method of ESR with microwave amplitude modulation is described in Appendix. A first derivative curve of microwave power dependence of ESR signal intensity can be obtained using this technique.

Contents

§1. Introduction

1.1 General introduction: outline and scope of this thesis

Continuous wave electron spin resonance (cw-ESR) used in physics and chemistry detecting paramagnetic defects and radicals has been applied to radiation dosimetry and dating (Ikeya, 1993). Defects and radicals produced by natural radiation such as alpha, beta and gamma rays are accumulated in minerals in a geological time scale. The total dose (TD) of natural radiation is obtained by additive dose method; aliquots of a sample are exposed to successive artificial doses and the enhancement of ESR signal intensity is fitted to a growth curve and the extrapolation of the growth curve to zero ordinate gives TD. The age is determined by dividing TD by the annual dose rate.

The most serious problem in ESR dating is that the signal used for ESR dating is interfered by other signals due to paramagnetic impurities such as transition metal and rare earth ions and it makes ESR dating impossible. A typical one is Mn^{2+} in calcite ($CaCO_3$). A pulsed ESR technique has progressed recently and electron spin echo (ESE) gives important information about the relaxation processes of electron spins in a substance. One advantage is to select a particular signal using the relaxation time from the complex overlapping signals. However, no work has been made to apply ESE technique to dating and dosimetry. The aim of this thesis is to study the ESE of paramagnetic defects in minerals such as $CaCO_3$, SiO_2, $NaHCO_3$, $CaSO_4 \cdot 2H_2O$ and $BaSO_4$ for the development of the ESE dating and dosimetry.

In this chapter, the principles of the methods, crystal structures of minerals and point defects in minerals are reviewed. Experimental results on paramagnetic defects produced by radiation in $CaCO_3$ (aragonite and calcite) are described in the first half of Chapter 2. In the latter half of this chapter, the results of the pulsed ESR measurements are described. The ESE intensity of CO_2^- in aragonitic shell is enhanced by the additive gamma-irradiation giving a paleodose. This is the first demonstration which obtains a paleodose by ESE measurements. In Chapter 3, E' centers in quartz (SiO_2) irradiated by alpha-rays (He^+-beam), neutrons, and those produced by gamma-irradiation after crushing as well as in

gamma-irradiated silica glass are investigated using cw/pulsed ESR. The obtained phase relaxation times, T_2, are compared with the line-widths and the ratios of homogeneous to inhomogeneous broadening obtained from the microwave power dependency. In Chapter 4, results of pulsed ESR measurements of evaporites such as $NaHCO_3$ (nahcolite), $CaSO_4 \cdot 2H_2O$ (gypsum) and $BaSO_4$ (barite) are discussed. A new technique is proposed to estimate a paleodose using the dose-dependence of the phase relaxation time. ESR with a microwave amplitude modulation is described in Appendix. A first derivative curve of microwave power dependence of ESR signal intensity can be obtained using this technique. The signal of CO_2^- in hydroxyapatite (a fossil shark tooth) and E' centers in quartz are measured for a demonstration purpose.

1.2 Basic principle of cw-ESR and pulsed ESR

Electron spin resonance is a microwave absorption spectroscopy which detects the magnetic resonance of unpaired electron spins. Electron magnetic moment appears in the substances containing transition metals, in the conduction electrons, in the paramagnetic molecules and so on. Addition to the above matters, chemical impurities (donors and acceptors) and physical impurities (lattice defects) also show the paramagnetism. The color centers in the ionic crystals are the typical one among paramagnetic lattice defects.

Magnetic moment of electron spin, μ_s occurs in the opposite direction to the spin momentum, S. This is expressed as

$$\mu_S = -g\beta S ,\tag{1-1}$$

where g is the g-factor (2.0023 for a free electron) and β is the Bohr magneton (9.2741×10^{-21} erg·G^{-1}). The hamiltonian, H_s of an electron in a magnetic field, H_0 is written as

$$H_s = -\mu_S \cdot H_0 = g\beta S \cdot H_0 .\tag{1-2}$$

Eigen values of the hamiltonian, H_s are $E_1 = +\frac{1}{2}g\beta H_z$ and $E_2 = -\frac{1}{2}g\beta H_z$ where the direction of the quantization is the z-axis. The transition between the two Zeeman levels can be induced by an electromagnetic wave with the frequency of ν. The condition of the resonance absorption of the electromagnetic wave is obtained as

$$\Delta E = E_1 - E_2 = g\beta H_z . \qquad (1-3)$$

In most cases, the g-factors deviate slightly from that of free electron due to the contribution of the orbital angular momentum via the spin-orbit interaction.

Figure 1-1 shows the behavior of magnetic moments in the rotating coordinate system during Hahn's microwave pulse sequence. The system is rotating around the external magnetic field, H_0, with a frequency of $\omega = \gamma H_0$. When we apply the microwave pulse with a frequency of ω and an amplitude of H_1, the magnetic moment, M, will be turned by the angle,

$$\theta = \gamma H_1 t_p , \qquad (1-4)$$

where t_p is the length of the pulse. The microscopic magnetic moments which were turned by the angle of $\pi/2$ start defocusing in x' - y' plane after the pulse because of different Larmor precession frequency resulting in free induction decay (FID). Magnetic moments refocus to produce an echo after the π-pulse.

The echo-intensity decays as the interpulse-time, τ, increases because the stochastic change of dipole interactions of the magnetic moments with each other and with magnetic nuclei interferes the complete refocusing. The decay constant is called phase relaxation time, T_2, and the decrease of echo-intensity is expressed as,

$$I = I_0 \exp(-2\tau / T_2) . \qquad (1-5)$$
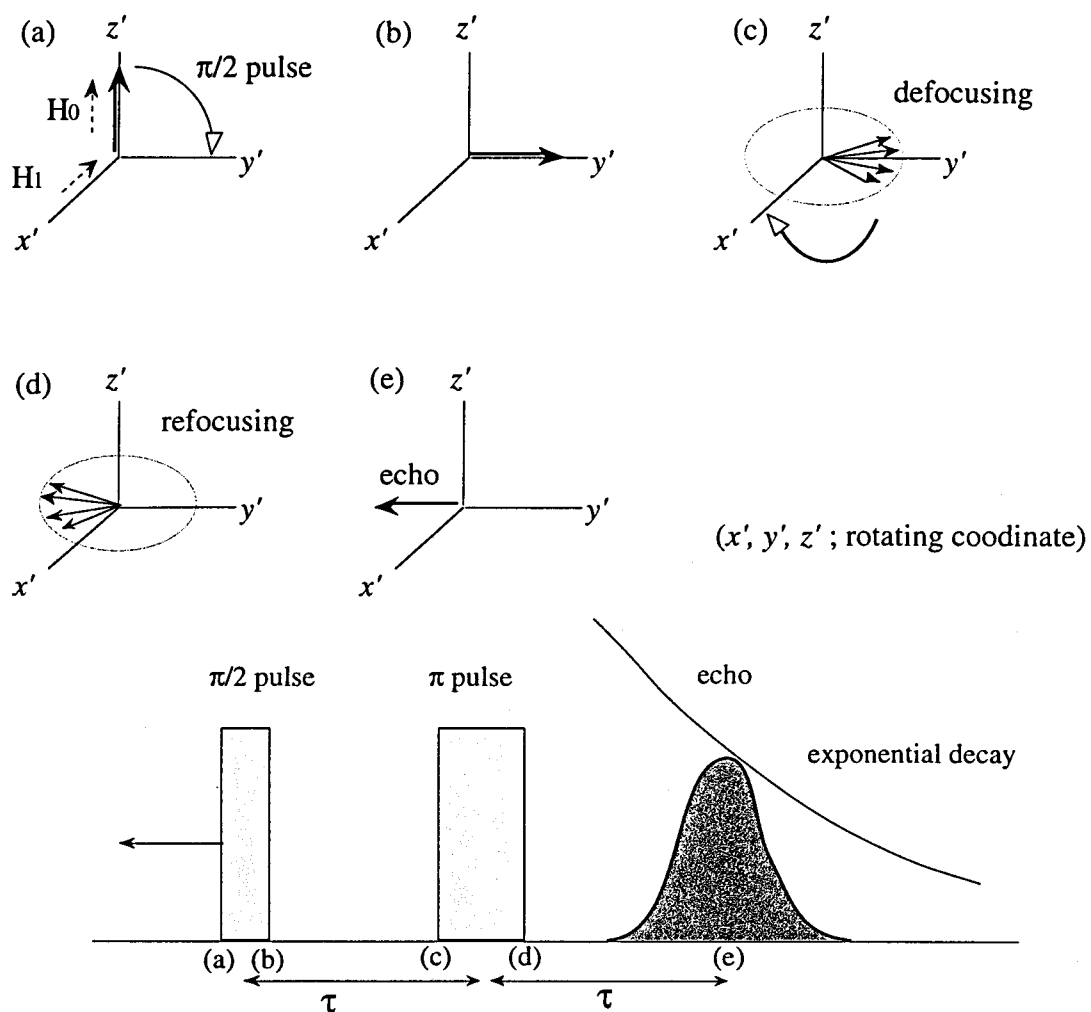
3

Fig. 1-1: Behavior of microscopic magnetic moments in the rotating coordinate system: (a) and (b) rotation of the total magnetic moment to the y'-axis by $\pi/2$-pulse, (c) defocusing of microscopic magnetic moments and rotation of magnetic moments by 180 ° during the second π-pulse, (d) refocusing of magnetic moments and (e) formation of the electron spin echo.

4

1.3 Principle of ESR dating

Natural ionizing radiation (alpha-, beta- and gamma-rays from radioactive elements, and cosmic rays) produces unpaired electrons in minerals, and electron excess centers and electron deficient centers are formed when the unpaired electrons are trapped by lattice defects or chemical impurities. The amount of unpaired electrons (defects/radicals) in a mineral increases as it ages. We can know the age of the minerals by measuring the amount of ESR absorption of the radiation sensitive centers. An ESR age is defined as the period since the zeroing processes of the defects/radicals such as mineralization, thermal annealing and optical or mechanical bleaching.

In ESR dating, the additive dose method is used in order to decide the total amount of radiation accumulated in the sample. Sample is separated into some aliquots and irradiated by gamma-rays artificially with various doses. Total dose (*TD*) is obtained by extrapolation of signal enhancement curve to the zero ordinate. This enhancement curve is fitted to the saturation curve which is expressed as follows:

$$I = I_\infty \left(1 - e^{-a(Q+TD)} \right) , \tag{1-6}$$

where I is a signal intensity, I_∞ is a saturation value of intensity and Q is a dose of artificial dose. An ESR age, T, is derived from the following relationship:

$$TD = \int_0^T D(t) \mathrm{d}t , \tag{1-7}$$

$$D(t) = kD_\alpha + D_\beta + D_\gamma , \tag{1-8}$$

where $D(t)$ is the time-dependent dose rate and k is the effective efficiency of alpha-rays relative to gamma-rays. $D(t)$ is evaluated from the concentrations of radioactive elements (^{238}U-series, ^{232}Th-series and ^{40}K) in the sample and its immediate surroundings.

1.4 Mineralogy of CaCO₃ (aragonite and calcite), SiO₂ (α-quartz), NaHCO₃ (nahcolite), CaSO₄·2H₂O (gypsum) and BaSO₄ (barite)

Aragonite (CaCO$_3$, orthorhombic, a = 4.96 Å, b = 7.97 Å and c = 5.74 Å) is a mineral which composes some shells, pearls, corals and marine mud of biological origin. In various types of CaCO$_3$, coral (aragonite) is especially important for ESR dating of sea-level movements, because a coral reef formation is controlled by relative sea-level movements. Aragonite has a greater density and hardness, and a less distinct cleavage than calcite. The structure of aragonite is shown in Fig. 1-2. The CO$_3^{2-}$ ions and the pseudo-hexagonal layers of Ca^{2+} are arranged parallel to (001) plane and the distance between the Ca^{2+} plane and CO$_3^{2-}$ is c/6.
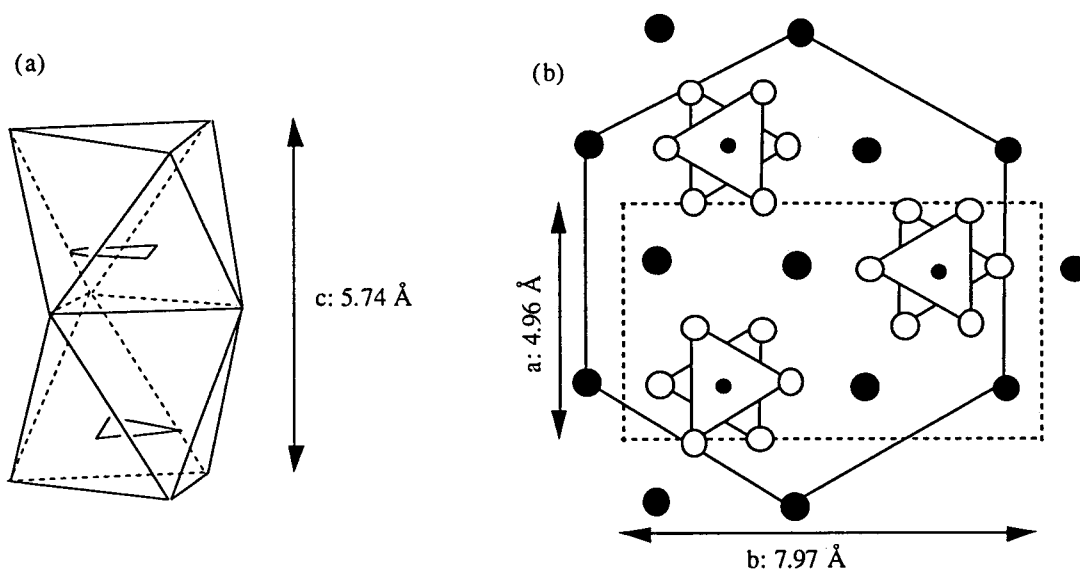
Fig. 1-2: The crystal structure of aragonite (CaCO$_3$). The CO$_3^{2-}$ is arranged in an octahedron formed by Ca^{2+} ions. (after Kai, 1992)

Calcite is the only thermodynamically stable form of calcium carbonate at room temperature and one atmospheric pressure. It constitutes most limestone, marble and cave deposits. The structure is rhombohedral symmetry (Fig. 1-3, shown by dotted line) and show a perfect rhombohedral cleavage consistent with rhombohedron shown by solid line in Fig. 1-3. The hexagonal unit cell (a = 4.99 Å and c = 17.06 Å) is also defined.
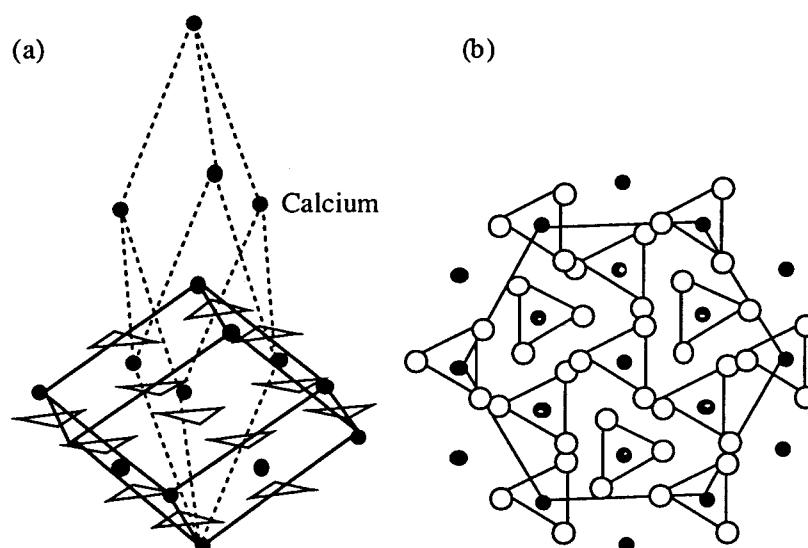
Fig. 1-3: The crystal structure of calcite. The true unit cell is shown by dashed lines and the cleaved cell by solid line. (after Kai, 1992)

Quartz (SiO_2, α-quartz) is one of the most common rock-forming minerals. α-quartz has a trigonal structure ($a = 4.91$ Å and $c = 5.42$ Å, shown in Fig. 1-4) and is stable at atmospheric pressure and temperature up to 573 °C. One oxygen has two bonds; the short bond is 1.607 Å and the long bond is 1.611 Å.

7

(a)   (b)
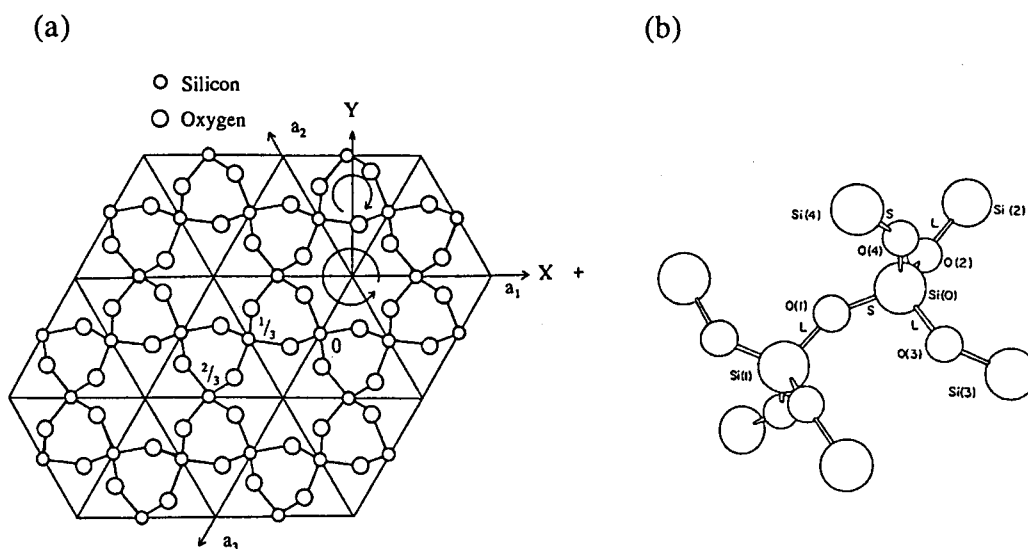
Fig. 1-4: The crystal structure of α-quartz. (a) Projection onto the plane perpendicular to *c*-axis (after Toyoda, 1992; originally after Weil, 1984) and (b) a part of atomic disposition (after Rudra and Flowler, 1987).

Nahcolite ($NaHCO_3$, monoclinic, $a = 3.51$ Å, $b = 9.71$ Å, $c = 8.05$ Å and $\beta = 111°51'$) is one of the evaporites. The evaporated nahcolite deposits in the present semi-arid lake and dune stratigraphy were formed in Quaternary wet/dry seasons. The structure is shown in Fig. 1-5. Each sodium ion is arranged in a slightly distorted octahedron of six oxygen atoms. It consists of layers of anions alternating with cationic layers approximately parallel to the $10\overline{2}$ planes.

8
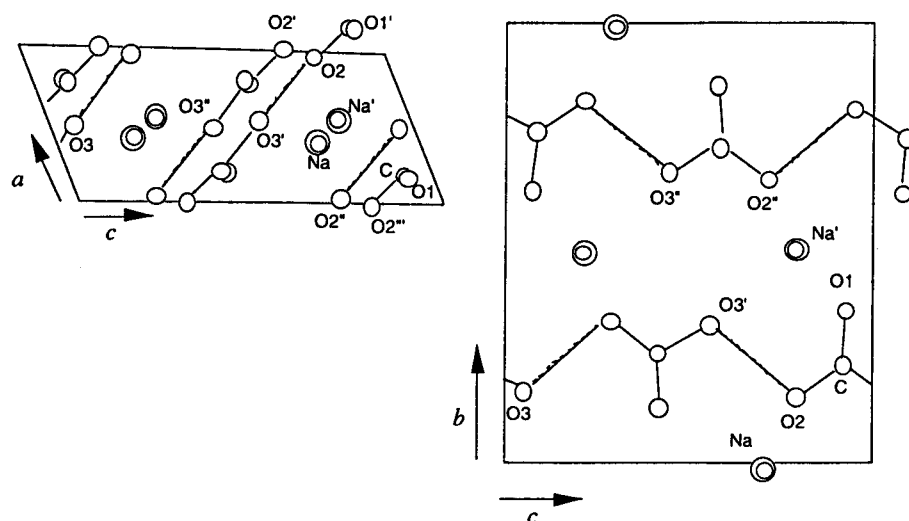
Fig. 1-5: Projection of the nahcolite down the a and b axes. (after Sass and Scheuerman, 1962)

Gypsum ($CaSO_4 \cdot 2H_2O$, monoclinic) is the most common sulfate minerals, which often occurs as evaporite deposits. The structure projected to the perpendicular to the c- and a-axes of the unit cell is shown in Fig. 1-6.
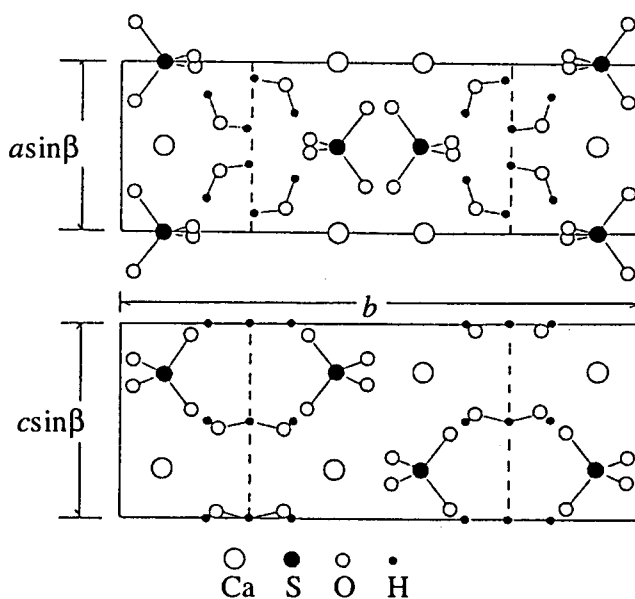
Fig. 1-6: Projection of the gypsum down the c and a axes. (after Deer et al., 1966)

9

Barite ($BaSO_4$, orthorhombic, $a = 8.88$ Å, $b = 5.45$ Å, $c = 7.15$ Å) is a evaporite mineral that often occurs as "desert rose". The structure is shown in Fig. 1-7. It consists of a divalent cation of Ba^{2+} and a divalent tetrahedral molecular anion, SO_4^{2-}.
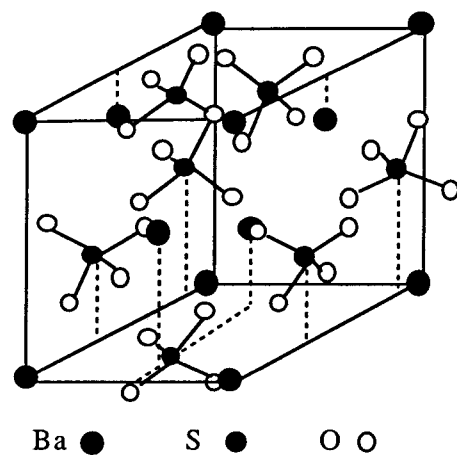
Ba ●   S ●   O ○

Fig. 1-7: The crystal structure of barite. (after Deer *et al.*, 1966)

1.5 Typical radicals in $CaCO_3$ (aragonite and calcite), SiO_2 (quartz), $NaHCO_3$ (nahcolite), $CaSO_4 \cdot 2H_2O$ (gypsum) and $BaSO_4$ (barite)

$CaCO_3$ (Aragonite and calcite) (see Table 1-1)

Four signals termed A, B, C and D are ordinary observed in powdered calcium carbonate. Signal A (g_{iso} = 2.0057) is observed in both aragonite and calcite. ESR intensity of this signal is not enhanced by additive gamma-irradiation, but increased by heating (Wintle, 1978). Kai and Miki, 1992 suggested that it may be attributed to sulfite-associated radical, SO_2^-. Signal B (g_{iso} = 2.0031) is observed only in aragonite. This signal is attributed to the SO_3^- radical from the study of synthetic aragonite doped with SO_3^{2-} ions (Kai and Miki, 1992). Signal C (g_{iso} = 1.9973) has been used for ESR dating and identified as isotropic CO_2^- radical (Debuyst et al., 1991). The orthorhombic CO_2^- takes place with this signal at low temperature below 200 K. Signal D (g_{yy} = 1.9973) is a part of orthorhombic CO_2^- with the g-factors of g_{zz} = 2.0016, g_{xx} = 2.0032 and g_{yy} = 1.9973 which is reported in both calcite (Marshall et al., 1964) and aragonite (Katzenberger et al., 1989).

Table 1-1: Typical radicals reported for $CaCO_3$. (after Ikeya, 1993)

Species	Material	g_{zz}	g_{xx}	g_{yy}	Notes	Ref.
CO_2^- iso.	calcite	g_{iso} = 2.0008			A_{iso} = 14.9 mT (^{13}C)	1
	aragonite	g_{iso} = 2.0007				2
CO_2^- axial	calcite	$g_{//}$ = 2.0033	$g_\perp$ = 1.9996		α-irradiation	3
CO_2^- ortho.	calcite	2.0016	2.0032	1.9973		4
CO_3^- ortho.	calcite	2.0056	2.0100	2.0180		1
SO_2^- iso.	aragonite	g_{iso} = 2.0060				5
SO_3^- iso.	aragonite	g_{iso} = 2.0034				5
SO_3^- axial	calcite	$g_{//}$ = 2.0024	$g_\perp$ = 2.0038		A = 13.2 mT (^{33}S)	5
SO_3^- ortho.	aragonite	2.0042	2.0038	2.0025	A = 11.4 mT (^{33}S)	5

Reference: 1) Debuyst et al,. 1991; 2) Miki and Kai, 1990; 3) Debuyst et al., 1990; 4) Marshall et al,. 1964; 5) Kai and Miki, 1992.

SiO_2 (Quartz and silica glass) (see Table 1-2)

E' center with the g-factors of 2.0003, 2.0005 and 2.0018 (Jani et al., 1983), which is an unpaired electron at an oxygen vacancy, is the most typical paramagnetic defect in crystalline quartz and silica glass detected by ESR. Aluminum hole center is also a common center observed. Its electron structure is attributed to $[AlO_4]^0$ (O'Brien, 1955). Its signal is split by the hyperfine interaction with ^{27}Al ($I = 5/2$, 100 % abundance).

Table 1-2: Reported radicals for SiO_2. (after Ikeya, 1993)

Species	g_{zz}	g_{xx}	g_{yy}	Notes	Ref.
E_1' ($\equiv Si\cdot$)	2.0018	2.0005	2.0003		1
$[AlO_4]^0$	2.0602	2.0085	2.0020	$A_{av} = 0.6$ mT (^{27}Al)	2

Reference: 1) Jani et al., 1983; 2)Nuttal and Weil, 1981.

$NaHCO_3$ (Nahcolite) (see Table 1-3)

Ikeya and Kai, 1988 assigned the signal at $g_{//} = 2.0058$ and $g_\perp = 2.0183$ to CO_3^- which split into hyperfine doublet by a nearby proton nucleus. The signal with a dip at $g = 1.9975$ was associated with CO_2^-.

Table 1-3: Reported radicals for $NaHCO_3$. (after Ikeya, 1993)

Species	g_{zz}	g_{xx}	g_{yy}	Notes	Ref.
CO_3^- axial	$g_{//} = 2.0183$		$g_\perp = 2.0058$	$A_{av} = 1.1$ mT	1
CO_2^- axial	$g_{//} = 1.9975$		$g_\perp = 2.0025$	$A_{av} = 0.4$ mT	1

Reference: 1) Ikeya and Kai, 1988.

$CaSO_4\cdot2H_2O$ (Gypsum) (see Table 1-4)

Albuquerque and Isotani, 1982 reported four types of signals designed as A, B, C and D in X-ray irradiated natural crystal. On the other hand, Kasuya et

al., 1991a reported four types of signals termed as G1, G2, G3 and G4 which were observed in natural gypsum from deserts. Two signals G1 and G4 correspond to the B and A, respectively.

Signal G1 (g_{iso} = 2.0028-2.0042): The G1 center with an almost isotropic g-value was identified as SO_3^- from the hyperfine structure of ^{33}S (I = 3/2).

Signal G2 (g_{zz} = 2.0192, g_{xx} = 2.0084 and g_{yy} = 2.0088): This hole-type center corresponds to the signal at around g = 2.008-2.009 in powdered gypsum. ESR intensity of this signal is enhanced in synthetic gypsum doped with CO_3^{2-} and may be associated with CO_3^-, however, no hyper-fine structure was observed in ^{13}C-labeled sample. Another possible model is O_2^{3-}.

Signal G3 (g_{zz} = 1.9973, g_{xx} = 2.0029 and g_{yy} = 2.0027): The g-values suggest that G3 may be an electron-excess center. The signal at g = 2.003 in powdered gypsum corresponds to G3. The orthorhombic g-values for this signal agree well with that for CO_2^- in $CaCO_3$, so that G3 may be due to CO_2^- radicals.

Signal G4 (g = 1.999-2.008, A = 0.2-0.5 mT): Albuquerque and Isotani, 1982 identified this signal as the $O_2H\cdot$ radicals. This signal is hardly observed in powdered spectrum because of its broad linewidth.

Table 1-4: Typical radicals reported for $CaSO_4 \cdot 2H_2O$. (after Ikeya, 1993)

Species	g_{zz}	g_{xx}	g_{yy}	Notes	Ref.
G1: SO_3^- iso.	g_{iso} = 2.0028-2.0042			2.004 in powder	1,2,3
G2: CO_3^- or O_2^{3-}	2.0192	2.0084	2.0088	2.009 in powder	1,3
G3: CO_2^- ortho.	1.9973	2.0029	2.0027		1,3
G4: $O_2H\cdot$	g = 1.999-2.008			A = 0.2-0.5 mT	1
	2.003	1.999	2.088	A_{zz}=0.52, A_{xx}=0.21, A_{yy}=0.33mT	2

Reference: 1) Kasuya *et al.,* 1991a; 2) Albuquerque and Isotani, 1982; 3) Ikeda and Ikeya, 1992.

BaSO$_4$ (Barite) (see Table 1-5)

Ryabov *et al.,* 1983 identified the signal with g-factor of 1.9995, 2.0024 and 2.0031 as SO_3^- that was confirmed by hyperfine splitting of ^{33}S (I = 3/2,

0.76 %). In addition to that, a hole type center with g-factors of 2.0191, 2.0127 and 2.0103 is observed (Kasuya *et al.*, 1991b). No hyperfine splitting by ^{33}S is observed for the hole type center. A possible model is O_2^{3-} stabilized by as M^{3+} ion.

Table 1-5: Typical radicals reported for $BaSO_4$. (after Ikeya, 1993)

Species	g_{zz}	g_{xx}	g_{yy}	Ref.
SO_3^-	1.9995	2.0024	2.0031	1
O_3^{2-} (hole-type center)	2.0191	2.0127	2.0103	2

Reference: 1) Ryabov *et al.*, 1983; 2) Kasuya *et al.*, 1991b.

§2. CaCO$_3$ (Aragonite and Calcite)

2.1 Radicals produced by alpha and gamma irradiation

Determination of alpha/gamma effectiveness ratio, k-value, in causing defects is vitally important in both ESR and thermoluminescence (TL) dating. Artificial additive irradiation is generally carried out with gamma-rays from the source of ^{60}Co. Environmental radiation dose including alpha-, beta- and gamma-rays is necessary to be expressed in the term of equivalent gamma-dose on the additive dose method of dating. Considering the efficiencies of stable defect production by alpha-, beta- and gamma-rays, the effective annual dose rate may be written as eq. (1-8). Reported k-values for ESR dating is summarized in Table 2-1.

In previous works, radionuclides such as ^{210}Po (an alpha-emitter with a half-life of 138.38 days and a particle energy of 5.3 MeV) and ^{241}Am were doped in or coated on the samples to irradiate alpha-particles. A signal at $g = 2.0007$ (signal C) was usually used for determination of k-value for calcium carbonate.

Canniére et al., 1982, 1986, 1988 deal with calcium carbonate (calcite) in which ^{210}Po was doped. A comparison between ESR spectra of alpha- and gamma-irradiated synthetic calcite has been discussed. Canniére et al., 1986 reported various k-values for calcium carbonate (calcite and aragonite), carbonate apatite and tooth enamel. Debuyst et al., 1990 also used ^{210}Po and identified an axial CO$_2^-$ ($g_{//} = 2.0032$ and $g_\perp = 1.9995$) radical which is unique in alpha-irradiated calcite. Debuyst et al., 1991 have investigated gamma- and alpha-irradiated synthetic powdered calcite labelled with ^{13}C ($I = 1/2$).

A nuclear accelerator was also used as a source of alpha-particles (Lyons et al., 1985; Lyons, 1988; Lyons and Brennan, 1989, 1991). Use of nuclear accelerator has a number of advantages over the use of radionuclides such as the improvement of control in experiments and calibration. The k-value of 0.052 ± 0.006 for calcite was reported by Lyons and Brennan, 1991.

Table 2-1: The k-values so far reported for ESR dating.

Material	Signal	k-value	Reference
Speleothem	$g_C = 2.0007$	0.052 ± 0.006	Lyons and Brennan, 1991
Coral	$g_C = 2.0007$	0.06 ± 0.01	Grün and Schwarcz, 1988
Calcite	$g_C = 2.0007$	0.08 ± 0.01	Canniére *et al.*, 1986
Apatite	$g = 2.0026$	0.20 ± 0.02	Canniére *et al.*, 1986
Tooth enamel	$g = 2.0020$	0.15 ± 0.02	Canniére *et al,.* 1986
Mollusc	$g_C = 2.0007$	0.3 ± 0.1	Canniére *et al.*, 1986
	$g = 2.0019$	0.15 ± 0.05	Canniére *et al.*, 1986
Speleothem	$g = 2.0024$	0.17 ± 0.01	Canniére *et al.*, 1986

2.1.1 Experimental

$CaCO_3$ was synthesized following the procedure described in Wray and Daniels, 1957. Synthetic aragonite contains about 5 % of calcite while synthetic calcite is pure, as confirmed by X-ray diffraction studies. Aragonitic modern coral was crushed by a pestle to powder and the fraction under 106 μm was collected by sieving.

He^+-particles with the energy of 1.6-1.8 MeV produced by a Van de Graaff accelerator were irradiated in a vacuum of 4×10^{-5} torr. The emission of secondary electrons leaving from the target was prevented by adding a positive bias (~100 Volts) on the sample plate. The beam was focused to a spot of about 30 mm² and irradiation was made for a duration of 2 to 60 seconds with a dose of approximately 4×10^{12} to 8×10^{12} particles/cm²·s. A sufficient quantity of powder was used to give a sample density of approximately 20 mg/cm², which is thick enough to absorb all the energy of 1.6-1.8 MeV He^+. Gamma-irradiation was made at about 100 Gy/h from the source of ^{60}Co. The dose was calibrated with ESR using a commercial alanine dosimeter called Aminogrey (Hitachi Electric Wire Co.).

ESR measurements were made with a commercial X-band ESR spectrometer (JEOL, RE-1X and RE-2X), where the field modulation width was 0.02 mT at a modulation frequency of 100 kHz and the microwave power was 1 mW, 0.01

mW and 200 mW at room temperature. First-derivative spectra of ESR were sampled numerically and doubly integrated to obtain the intensity. The g-factors in this work were determined from hyperfine-lines of Mn^{2+} in MgO standard marker, and contain errors of ±0.0003.

2.1.2 Results and discussion

(a) Species of produced radicals

Aragonitic coral

ESR spectra of He$^+$- and gamma- irradiated aragonitic coral at the microwave power of 1 mW are shown in Fig. 2-1. Distinct difference in the spectra is observed. The simulated spectra are shown under the observed spectra and the parameters of ESR signals are tabulated in Table 2-2. No signal was observed in non-irradiated sample.

Orthorhombic signal with g_{xx} = 2.0036, g_{yy} = 2.0014 and g_{zz} = 1.9977 is dominant in He$^+$-irradiated coral. This signal is associated with an electron excess center from its g-factors and may be ascribed to CO$_2^-$ radicals because of its similarity of g-factors to those of the CO$_2^-$ in calcite (g_{xx} = 2.0032, g_{yy} = 2.0016 and g_{zz} = 1.9973, Marshall *et al.*, 1964). Isotropic CO$_2^-$ (signal C, g_{iso} = 2.0007, Debuyst *et al.*, 1991) was not observed in He$^+$-irradiated coral in this study.

Hole center with the g-factors of 2.0173, 2.0122 and 2.006-2.007 is also observed selectively in He$^+$-irradiated coral. Orthorhombic CO$_3^-$ in alpha-irradiated calcite with the g-factors of 2.0180, 2.0100 and 2.0056 is reported by Debuyst *et al.*, 1991. The peak which corresponds to g = 2.006-2.007 is too weak to observe with the microwave power of 1 mW, but is observable with higher microwave power. The g-factors of observed signal are similar to those of reported as CO$_3^-$ and saturation behavior towards microwave power for this signal is similar to that of orthorhombic CO$_3^-$ in alpha-irradiated calcite, so this signal may be ascribed to CO$_3^-$ radicals. Its peak height is very low due to the large anisotropy of g-factors while the concentration of spins obtained by doubly integrating the derivative spectrum is equal to that of CO$_2^-$. Isotropic SO$_2^-$ is the only sulfite-associated radical observed in He$^+$-irradiated coral. The peak-height

and the amount of this radical are very small.
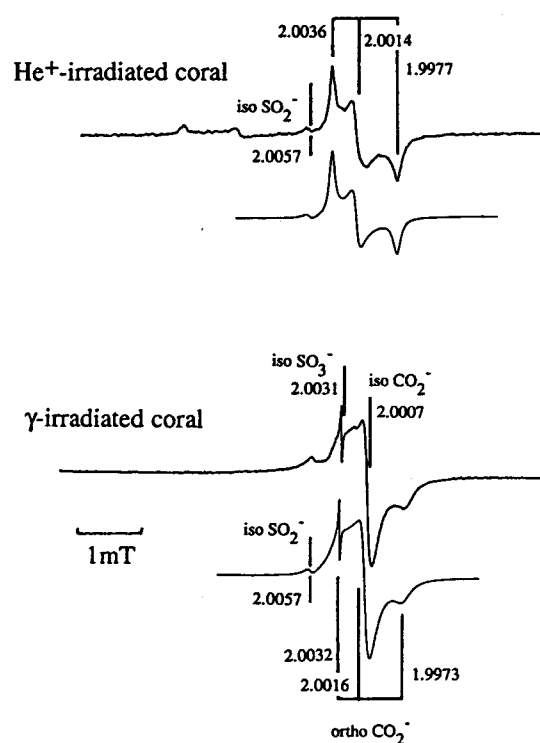
Fig. 2-1: cw-ESR spectra of He⁺- and gamma-irradiated powdered aragonitic coral. Microwave power was 1 mW. Orthorhombic CO_2^- radicals were dominant in He⁺-irradiated sample. The simulated spectra are shown under the observed spectra.

Carbonate-associated radicals observed in gamma-irradiated coral were isotropic CO_2^- and orthorhombic CO_2^-. Orthorhombic CO_3^- was not detected. Sulfite-associated radicals, iso. SO_2^-, iso. SO_3^- and ortho. SO_3^- were also observed in gamma-irradiated coral. The SO_3^- radicals saturate easily at high microwave power; therefore the measurement at low microwave power is preferable. The measurement at the microwave power of 0.01 mW gave the clear spectrum of SO_3^- radicals (Fig. 2-4). The amount of sulfite-associated radicals is very small

compared with that of carbonate-associated radicals for both He^+- and gamma-irradiated coral. The production of the sulfite-associated radicals seems to have little relation for both He^+- and gamma-irradiation.

Table 2-2: Observed radicals in aragonitic coral.

Species	g_{zz}	g_{xx}	g_{yy} *	Linewidth (mT)	Ratio	Simu. **
He^+-irradiation						
CO_2^- ortho.	2.0014	2.0036	1.9977	0.08	100	done
CO_3^- ortho.	2.006-7	2.0122	2.0173	0.15	60	done
SO_2^- iso.	$g_{iso} = 2.0057$			0.1	0.7	done
gamma-irradiation						
CO_2^- ortho.	2.0016	2.0032	1.9973	0.1	100	done
CO_2^- iso.	$g_{iso} = 2.0007$			0.15	50	done
SO_2^- iso.	$g_{iso} = 2.0057$			0.1	0.7	done
SO_3^- iso.	$g_{iso} = 2.0031$			0.02	0.3	done
SO_3^- ortho.	2.0039	2.0036	2.0022			

* The g-factors in this work were determined by hyperfine lines of Mn^{2+} marker and contain errors of ± 0.0003.
** Simulation were made to determine the approximate linewidth and abundance ratio of each radical from the powder spectra.

Synthetic aragonite

The ESR spectra of synthetic aragonite were very similar to these of aragonitic coral (Table 2-3, Fig. 2-2 and 2-4). Radical species were almost same as those in coral. The only difference is the ratio of the amount of each radical. The signal intensity of isotropic CO_2^- was relatively small compared to that of coral. The peak at $g = 2.0142$ and 1.9995 are due to calcite form because our synthetic aragonite sample contains some 5 % of calcite form.
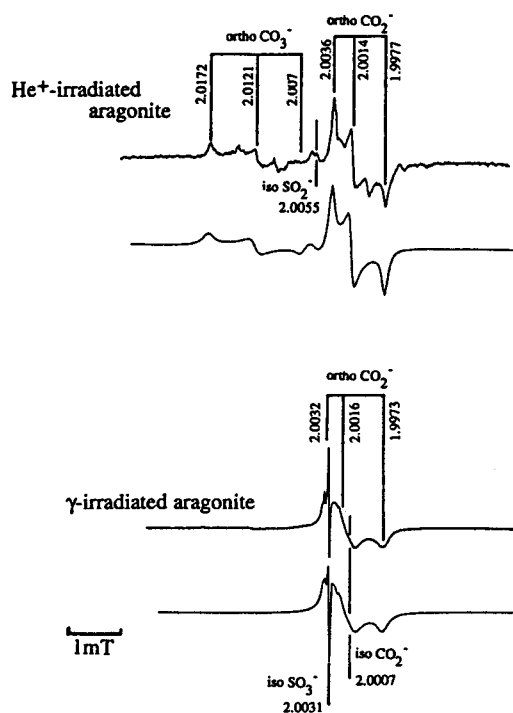
Fig. 2-2: cw-ESR spectra of He⁺- and gamma-irradiated synthetic aragonite measured at the microwave power of 1 mW.

Table 2-3: Observed radicals in synthetic aragonite.

Species	g_{zz}	g_{xx}	g_{yy}	Linewidth (mT)	Ratio	Simu.
He⁺-irradiation						
CO₂⁻ ortho.	2.0014	2.0036	1.9977	0.08	100	done
CO₃⁻ ortho.	2.006-7	2.0121	2.0172	0.15	60	done
SO₂⁻ iso.	g_{iso} = 2.0057			0.25	10	done
gamma-irradiation						
CO₂⁻ ortho.	2.0016	2.0032	1.9973	0.15	100	done
CO₂⁻ iso.	g_{iso} = 2.0007			0.2	10	done
SO₂⁻ iso.	g_{iso} = 2.0057			0.1	0.7	done
SO₃⁻ iso.	g_{iso} = 2.0031			0.005*	0.5	done
SO₃⁻ ortho.	2.0039	2.0036	2.0022	0.01*	1	done

* Measured at microwave power of 0.01 mW.

20

Synthetic calcite

Axial CO$_2^-$ was observed in He$^+$-irradiated synthetic powdered calcite (Fig 2-3, Table 2-4). This radical is unique to He$^+$-irradiated calcite. Signals at g = 2.0118 and 1.9974 are associated with the forbidden transition of Mn^{2+} that are also observed in non-irradiated sample. An axial SO$_3^-$ was clearly observed in gamma-irradiated calcite and barely in He$^+$-irradiated calcite at the low microwave power of 0.01 mW (Fig. 2-4).

Isotropic CO$_2^-$ was observed neither in He$^+$-irradiated aragonite nor calcite. It is reported that the radical may be associated with surrounding coordination water and water molecules may work as a stabilizer (Miki and Kai, 1990). The isotropic CO$_2^-$ may be produced efficiently around water by gamma-irradiation, while heavy particle irradiation induces radicals along the tracks forcibly and independently of the presence of water molecules.

In tracks, the crystalline lattice may be changed to an amorphous state and therefore defects would be indifferent to the original crystal phases. It is expected that He$^+$-irradiated aragonite and calcite show the same type of defects; however, their ESR spectra were different markedly. This indicates that radicals may be produced near the tracks by He$^+$-irradiation, but not in the amorphous parts of the crystal.
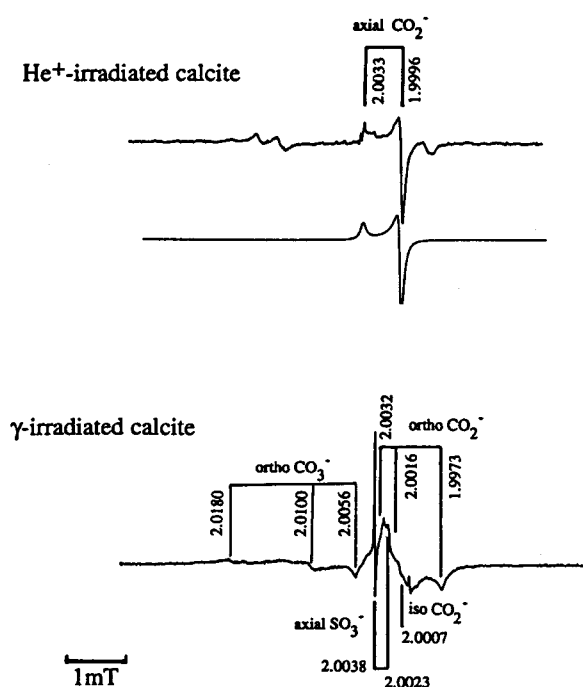
Fig. 2-3: Powder spectra of He⁺- and gamma-irradiated synthetic calcite. Microwave power was 1 mW. Axial CO_2^- radicals were observed in He⁺-irradiated calcite and the simulated spectrum is shown under the observed spectrum. Gamma-irradiated calcite presents a complex spectrum and simulation cannot give adequate similarity.

Table 2-4: Observed radicals in synthetic calcite.

Species	g_{zz}	g_{xx}	g_{yy}	Linewidth (mT)	Ratio	Simu.*
He⁺-irradiation						
CO_2^- axial	$g_{//} = 2.0033$	$g_\perp = 1.9996$		0.06		done
SO_3^- axial	$g_{//} = 2.0023$	$g_\perp = 2.0038$		-		
gamma-irradiation						
CO_2^- ortho.	2.0016	2.0032	1.9973	0.1		
CO_2^- iso.	$g_{iso} = 2.0007$			-		
CO_3^- ortho.	2.0056	2.0100	2.0180	0.15		
SO_3^- axial	$g_{//} = 2.0023$	$g_\perp = 2.0038$		0.005**		

* Simulation was not successful.
** Measured at microwave power of 0.01 mW.

22

a) γ-irradiated aragonite

b) He⁺-irradiated calcite

c) γ-irradiated calcite
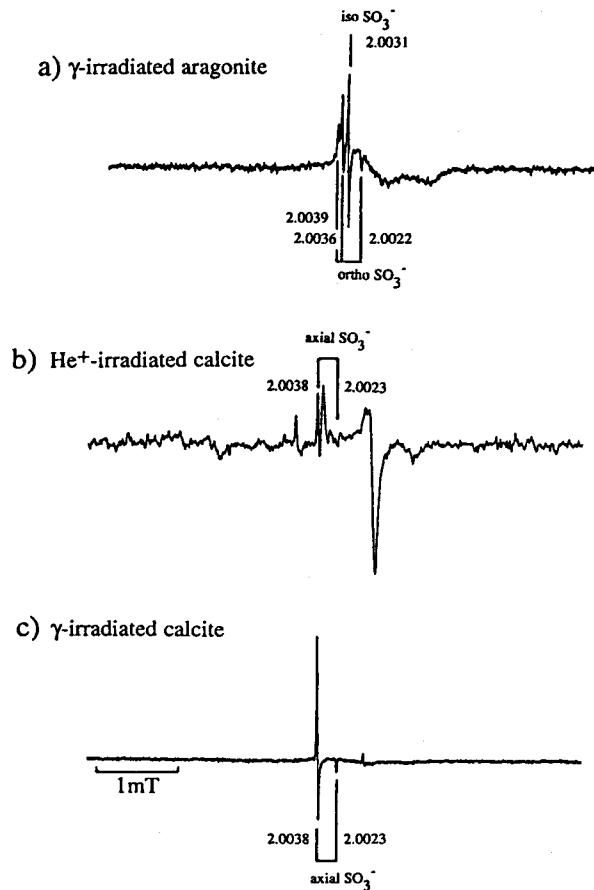
Fig. 2-4: ESR spectra measured at the microwave power of 0.01 mW. SO_3^- radicals can be observed clearly; a) isotropic and orthorhombic SO_3^- in gamma-irradiated synthetic aragonite, (b) axial SO_3^- in He⁺-irradiated calcite and (c) axial SO_3^- in gamma-irradiated calcite.

(b) Linewidth and saturation behavior

Anisotropic CO_2^- radicals in He⁺-irradiated aragonite and calcite have narrower linewidths than those in gamma-irradiated CaCO₃ (see Table 2-5). The linewidths were almost the same and independent of doses. The narrow linewidth

is against the expectation that radicals produced along the tracks are localized and strong interaction between spins causes broader linewidths of spectra (Ikeya *et al.*, 1992).

Table 2-5: Linewidth of anisotropic CO_2^- radicals in calcium carbonate.

Samples	anisotropy	linewidth (mT)
He^+-irradiated coral	orthorhombic	0.08
gamma-irradiated coral	orthorhombic	0.1
He^+-irradiated synthetic aragonite	orthorhombic	0.08
gamma-irradiated synthetic aragonite	orthorhombic	0.15
He^+-irradiated synthetic calcite	axial	0.06
gamma-irradiated synthetic calcite	orthorhombic	0.1

In addition, the saturation behavior upon increasing microwave power also seems to prove the weak spin-spin interaction on He^+-irradiated samples (Fig. 2-5). The anisotropic CO_2^- radicals in He^+-irradiated aragonite and calcite tend to saturate easily compared with these in gamma-irradiated samples.

In the case of homogeneous broadening, the linewidth of ESR absorption, $\Delta H_{\frac{1}{2}}$ (width at half the maximum intensity in gauss, lorentzian line), is in inverse proportion to the spin-spin relaxation time,

$$\Delta H_{\frac{1}{2}} = \frac{\hbar}{g\beta T_2} = \frac{0.568 \times 10^{-7}}{T_2} \ . \tag{2-1}$$

A linewidth of 0.1 mT (1 gauss) corresponds to a T_2 of about 60 ns. ESR signal intensity is maximum at a microwave power of

$$H_1 = \frac{1}{\gamma \sqrt{2T_1 T_2}} \ . \tag{2-2}$$

This implies that the orthorhombic CO_2^- in He^+-irradiated $CaCO_3$ is less

24

concentrated than those in gamma-irradiated $CaCO_3$ if the linewidth is homogeneously broadened. Presumably, CO_2^- would be produced around dislocations or another stabilizer in gamma-irradiated $CaCO_3$. On the other hand, He^+-irradiation would produce CO_2^- randomly along the alpha tracks but not in the amorphous part.
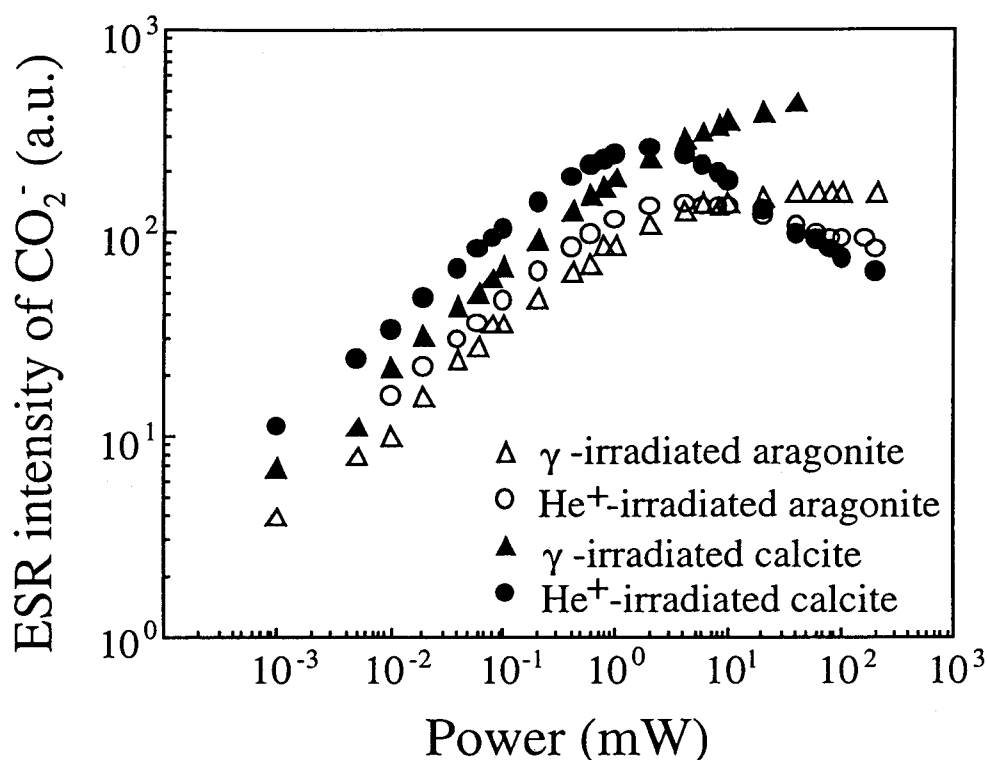
Fig. 2-5: Microwave power dependence of the signal intensities for orthorhombic CO_2^- radicals in gamma-irradiated synthetic aragonite (measured at $g = 1.9973$), He^+-irradiated synthetic aragonite (measured at $g = 1.9977$), gamma-irradiated synthetic calcite (measured at $g = 1.9973$) and for axial CO_2^- in He^+-irradiated synthetic calcite. Anisotropic signals of CO_2^- produced by gamma-irradiation saturate easily. Orthorhombic CO_2^- in coral behaved just like synthetic aragonite.

Inhomogeneous broadening due to superhyperfine interaction is also possible for CO_2^- produced by gamma-irradiation. If the broad linewidth for anisotropic CO_2^- produced by gamma-irradiation is due to superhyperfine structure (may be

due to protons of H_2O molecules), the signal intensity will not decrease at the region of saturation and observed behavior can be explained well. It is needed that only CO_2^- radicals produced by gamma-irradiation are near the nuclei which have nucleus spin of non-zero $(I = 1/2$ for proton) in this case. It is possible that CO_2^- radicals produced by gamma-irradiation are stabilized near the water molecules while He^+-irradiation forms the radicals having no relation with water along the alpha tracks.

(c) Thermal stability of anisotropic CO_2^- radicals

Thermal stability of the anisotropic CO_2^- radicals (orthorhombic ones for aragonite samples and gamma-irradiated calcite, and axial one for He^+-irradiated calcite) were examined by the method of isochronal annealing (15 min.) at 80 ~ 380 °C with the step of 20 °C (Fig. 2-6). Annealing curves for coral show almost the same behavior; however, the anisotropic CO_2^- radicals produced by He^+-irradiation in synthetic powdered samples (both aragonite and calcite) were stabler than those produced by gamma-irradiation.
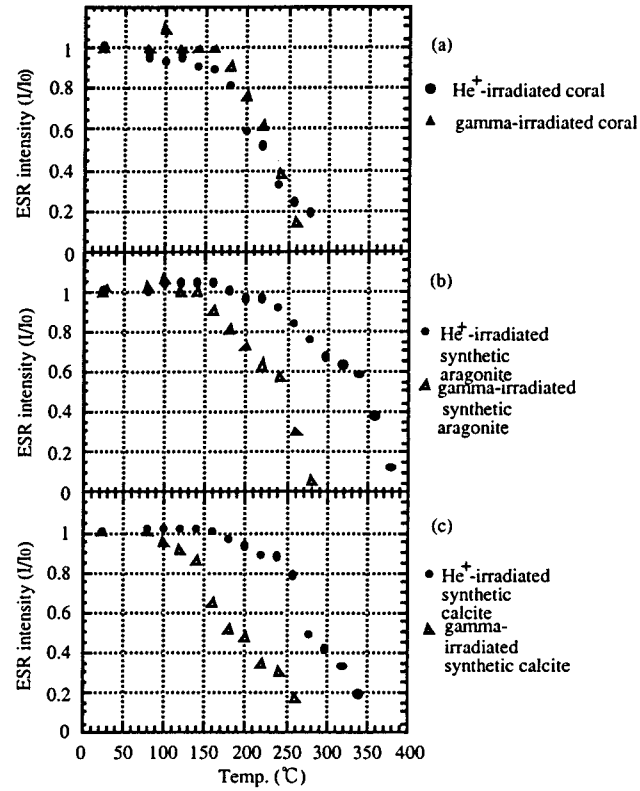
Fig. 2-6: Isochronal (15 min., 20 °C step) annealing curves of the ESR intensities of anisotropic CO_2^- radicals in (a) aragonitic coral, (b) synthetic aragonite and (c) synthetic calcite for He^+- and gamma-irradiation.

(d) Determination of alpha-ray effectiveness, k-value

Formation of defect

The formation of lattice defects induced by irradiation is described simply by the following differential equation

$$\frac{dn}{dx} = \frac{N_0 - bn}{N_0} \frac{G}{100} , \qquad (2\text{-}3)$$

where n is the number of lattice defects formed by irradiation, x dose in eV, N_0

total lattice points of the sample, G the yield per 100 eV and b the number of lattice points in the insensitive volume around a defect (not around a track).

The exact solution of eq. (2-3) with the boundary condition of $n = 0$ at $x = 0$ is written as

$$n = \frac{N_0}{b}\left\{1 - \exp\left(-\frac{b}{N_0}\frac{G}{100}x\right)\right\} = A\{1 - \exp(-Cx)\} . \qquad (2\text{-}4)$$

The G-value is obtained as

$$G = 100AC . \qquad (2\text{-}5)$$

If doses are low enough to ignore the saturation, eq. (2-4) can be simplified to

$$n = \frac{G}{100}x . \qquad (2\text{-}6)$$

The alpha/gamma effectiveness ratio, k-value is written by G-values of alpha- and gamma-rays as

$$k = \frac{G_\alpha}{G_\gamma} = \frac{A_\alpha C_\alpha}{A_\gamma C_\gamma} . \qquad (2\text{-}7)$$

Accelerator He⁺-irradiation as alpha-rays

In the case of gamma-irradiation, saturation is uniform in the entire sample volume. An optional aliquot can represent the entire sample through normalization with mass. On the other hand, the range of alpha-particles is about 2 mg/cm² (7.4 μm) at 2 MeV for calcium carbonate. Incident particles affect only the surface layer and the surface easily reaches a saturation concentration. Dose calculated from the total energy deposited in the sample divided by the total mass of the sample should not be adopted.

Irradiation with He^{2+} ions may be ideal because a-particles in ^{238}U-series

disintegration have the same structure as the nuclei of He atoms. The second ionization energy of a He atom is 54.4 eV while incident energy is 1.6-1.8 MeV, and hence, the difference between He^+ and He^{2+} is quite small; therefore, the same radiation effects as with He^{2+} are expected.

There is an obvious difference between the species of defects produced by gamma- and He^+-irradiation. It is not suitable to determine the k-value from the growth of the peak height of a particular signal. Distribution of incident energy is different and the linewidth of the signal may differ. Determination of k-value was made using the absolute number of produced paramagnetic defects, i.e., the area of the absorption curve.

Obtained G-values and k-values

Coral: The k-value of 0.0020 ± 0.0008 for 1.8 MeV He^+-particles was obtained from the parameters of the growth curves. Calculated G-values are 0.0014 ± 0.0001 and 0.71 ± 0.28 paramagnetic radicals per 100 eV for He^+-irradiated coral and gamma-irradiated, respectively.

Synthetic aragonite: G-values of 0.0041 ± 0.0008 and 0.27 ± 0.03 were obtained for 1.6 MeV He^+-irradiation and gamma-irradiation. The k-value was decided as 0.015 ± 0.005.

Synthetic calcite: The growth curve for 1.6 MeV He^+-irradiated calcite was already saturated, so the G-value could not obtained for this sample. Obtained G-value for gamma-irradiation was 0.30 ± 0.11. Obtained G-values and k-values are tabled in Table 2-6.

Table 2-6: Obtained G and k-values for calcium carbonates.

Samples	G_α	G_γ	k
Aragonitic coral	0.0014 ± 0.0001 (1.6 MeV)	0.71 ± 0.28	0.0020 ± 0.0008
Synthetic aragonite	0.0041 ± 0.0008 (1.8 MeV)	0.27 ± 0.03	0.015 ± 0.05
synthetic calcite	-	0.30 ± 0.11	-

Two of synthesized samples contain Mn^{2+} as impurity and a Mn^{2+} ion replace a Ca^{2+} ion in the lattice of calcium carbonate. The insensitive volume (about 10 atomic distance) is created around a Mn^{2+} ion in calcium carbonate. An electron-hole pair which is formed in the volume recombines as soon as it is created and its energy is transformed to Mn^{2+} ion followed by phosphorescence of orange-yellow. The small G_γ-values for synthesized samples against that for coral may be due to the insensitive volume of Mn^{2+} ions. The reason for the difference in G_α is not cleared in this study.

ESR intensity per alpha-particle is in proportion to the range of the incident particles (Lyons, 1988, Lyons and Brennan, 1989). Range per energy increases as the energy of a particle increases. The high-energy particle can produce defects more efficiently than the low-energy particle for the same deposition energy on the sample. Most natural alpha-particles have the energy of 4-6 MeV. The correction factor for a 1.6-1.8 MeV alpha-particle is calculated as follows:

$$\frac{\Sigma Range/\Sigma Energy\ for\ U-238\ series}{Range/Energy\ for\ 1.6\ (1.8)\ MeV}. \tag{2-8}$$

This factor for $CaCO_3$ is 1.34 in equilibrium and no-radon-loss case, and 1.24 in the case of 100 % radon loss. Thus, the k-value of 0.0027 ± 0.0011 and 0.021 ± 0.007 in equilibrium for ESR dating was calculated for aragonitic coral and synthetic aragonite, respectively (see Table 2-7).

Table 2-7: Calibrated k-values for calcium carbonate for ESR dating.

Samples	k
Aragonitic coral	0.0027 ± 0.0011
Synthetic aragonite	0.021 ± 0.007

2.2 Pulsed ESR measurements

2.2.1 Experimental

Pulsed ESR measurements at the X-band frequency were also done using a commercial spectrometer (JEOL, JES-PX1050) with 20 W traveling wave tube amplifier (TWTA), where the Hahn's spin-echo method was applied. Two series of pulse sequence with following phases were applied where -π/2 and -π indicate the π/2 and π pulses with the microwave phase reversed.

(+π/2)----(-π)..................(A)
(-π/2)----(+π)..................(B)

The subtraction of two echo spectra of (A) and (B) gives only the signal of the spin-echo while the ringing of pulsed microwave and unexpected signals on background is reduced effectively by the subtraction.

2.2.2 Results and discussion

(a) Selective detection of orthorhombic CO$_2^-$

Modern coral was subjected to extra-heavy gamma-irradiation with the dose of about 30 kGy for pulsed ESR measurements. Hahn's two-pulse spin echo intensity is plotted as a function of magnetic field with a solid line (a) in Fig. 2-7, where the time between the first pulse and the second pulse, τ, is 400 ns. A broken line (b) shows a continuous-wave ESR spectrum measured at microwave power of 1 mW, which contains signals of both orthorhombic and isotropic CO$_2^-$, while the dotted line (c) shows a simulated signal of solely the orthorhombic one. The electron spin echo (ESE) spectrum is similar to that of the solely orthorhombic one. This indicates that a spin-spin relaxation time, T_2, of the isotropic one is shorter than that of the orthorhombic one. We can separate the signals using a pulsed ESR technique when τ is sufficiently long, while the selective measurement of orthorhombic CO$_2^-$ is difficult for the cw-ESR spectra.
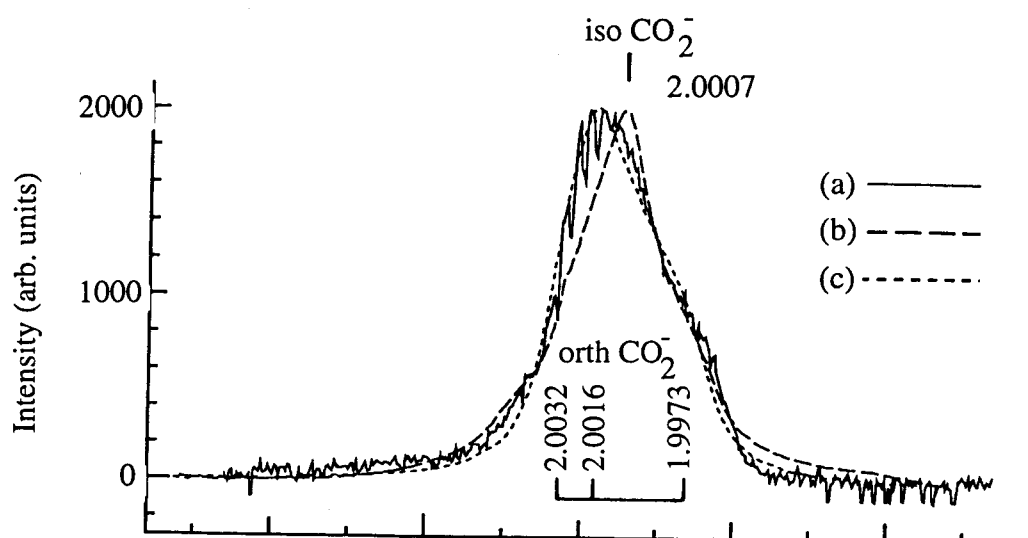
Fig. 2-7: (a) The field sweep electron spin echo (ESE) spectrum for gamma-irradiated coral (solid line), (b) continuous-wave ESR (cw-ESR) spectrum with both isotropic and orthorhombic CO_2^- (broken line) and (c) calculated cw-ESR spectrum of only orthorhombic CO_2^- (dotted line).

Figure 2-8 shows the ESE decay of CO_2^- with the spin-spin relaxation time of 1.25 ± 0.04 μs assuming a single exponential decay. No modulation was visible on ESE decay. The single exponential decay fitting does not give sufficient agreement, while a fitting to double exponential decay gives T_2 of 0.82 ± 0.04 μs (87 % in abundance) and 6.8 ± 0.5 μs (13 %). The obtained T_2 (assuming single exponential decay) corresponds to a homogeneous linewidth of 0.004 mT. This width is considerably narrow compared with observed widths of 0.06-0.08 mT for CO_2^- produced by He^+-irradiation and 0.1-0.15 mT for gamma-irradiation. The absorption line of CO_2^- produced by gamma- and He^+-irradiation may be inhomogeneously broadened. The degree of broadening is smaller than that for gamma-irradiation and this is reflected in the microwave saturation behavior.

A fossil shell collected at Alaska was also measured. The ESE decay curve is shown in Fig. 2-8. Single exponential fitting gives a spin-spin relaxation time

of 1.58 ± 0.02 μs, slightly longer than that of coral. The local concentration of defects in coral may be higher than that in fossil shell.
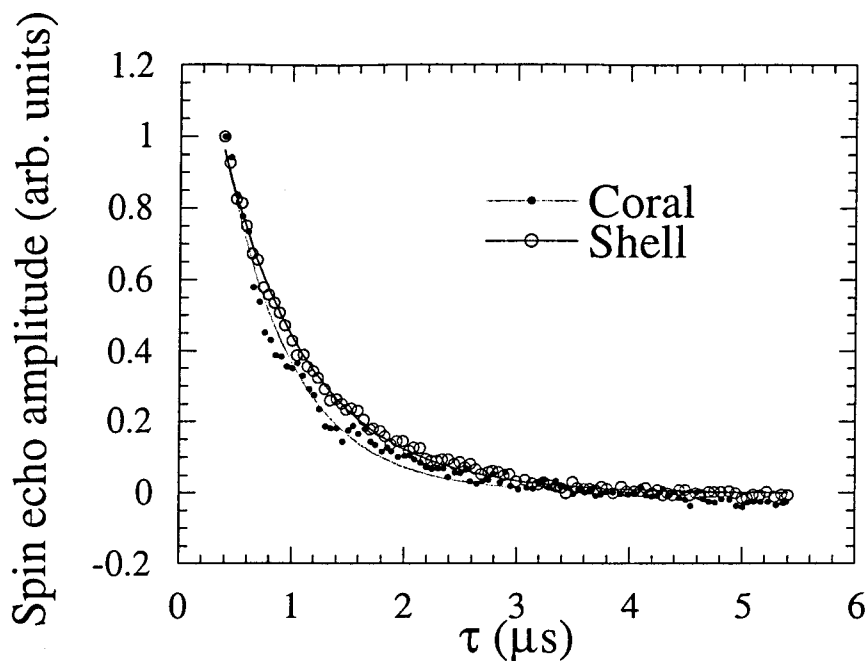

Fig. 2-8: Two-pulse ESE signal decay for orthorhombic CO_2^- in gamma-irradiated modern coral and fossil shell.

(b) Estimation of a total dose and an age by spin echo method

Figure 2-9 shows a cw-ESR spectrum and a field sweep ESE spectrum of the non-irradiated fossil aragonitic shell collected at Alaska. The orthorhombic signal due to CO_2^- with anisotropic g-factors of $g_x = 2.0032$, $g_y = 2.0016$ and $g_z = 1.9973$ is the main species for both cw-ESR and ESE measurements. A weak signal of isotropic CO_2^- (rapidly tumbling in the lattice as to give an averaged isotropic g-factor of $g_{iso} = 2.0007$) might superpose on the signal of orthorhombic one in the cw-ESR spectrum. ESR dating has been made using this signal at $g = 2.0007$. Presence of H_2O molecule was speculated from various studies including the results of electron-nuclear double resonance (ENDOR) and thermogravimetric analysis (TGA) by Callens *et al.*, 1994. Anisotropic signal of CO_2^- was formed

on the other hand at the normal lattice especially by alpha-irradiation. The selective detection of the orthorhombic CO$_2^-$ is difficult for cw-ESR measurements because the signal intensity of the isotropic one hardly saturates at a high microwave power (~200 mW), while the orthorhombic one saturates at a microwave power of about 10 mW. The signal of the isotropic CO$_2^-$ was effectively removed for the spin-echo measurement. The selective detection of the orthorhombic one is also expected in this study.
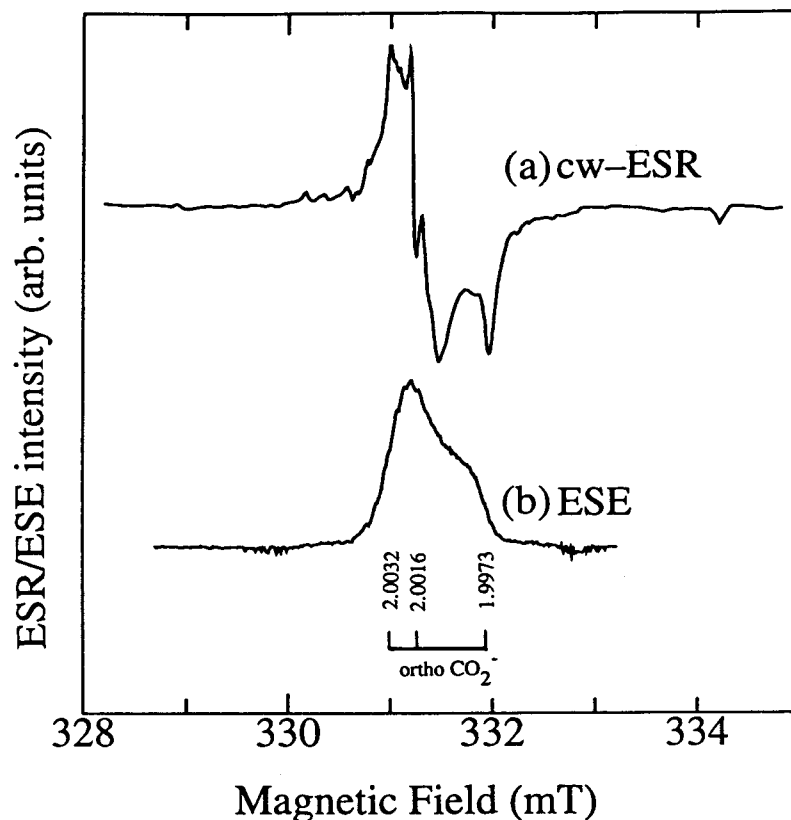

Fig. 2-9: (a) cw-ESR and (b) field sweep ESE spectra for fossil shell. Orthorhombic CO$_2^-$ was the main species detected.

Figure 2-10 shows the enhancements of the spin echo intensities of the orthorhombic CO$_2^-$ against additive gamma dose for both ESE and cw-ESR measurements. Data were fitted to a linear function and the total doses of 940 ±

720 Gy and 930 ± 170 Gy were obtained by ESE and cw-ESR, respectively. The precise estimation of the total dose by ESE is difficult because of the poor S/N ratio under present circumstances. However, the obtained total dose by ESE was consistent with that by cw-ESR within the experimental error. The total doses correspond to the ages of 0.76 ± 0.58 Ma and 0.75 ± 0.14 Ma, respectively with an annual dose of 1.24 mGy/a estimated from the content of 2.52 ppm of ^{238}U, 10.23 ppm of ^{232}Th and 2.06% of K_2O in the sediment considering the radiation equilibrium. The result indicates that ESE can also be useful for dating.
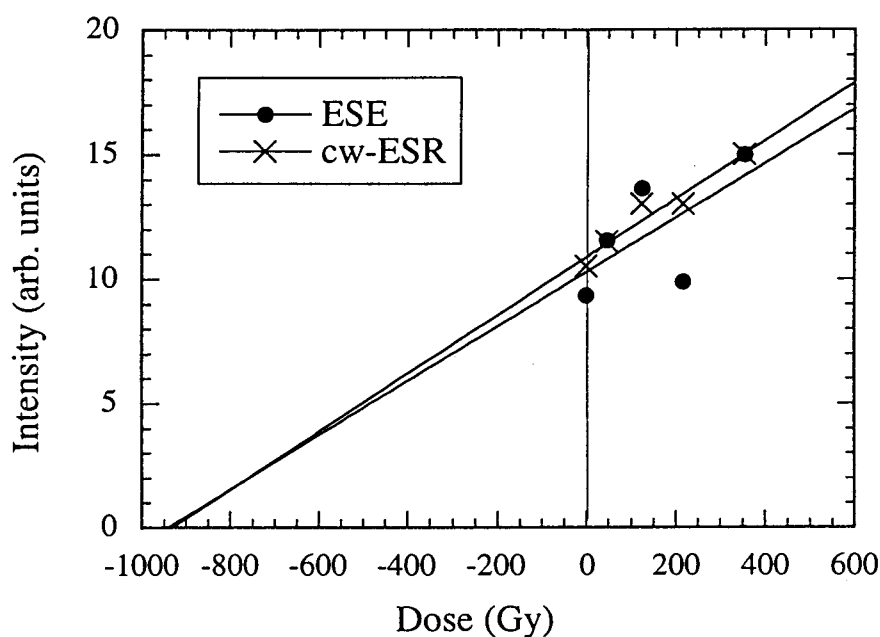

Fig. 2-10: The signal intensities of orthorhombic CO_2^- plotted as a function of additive dose for ESE and cw-ESR measurements. Total doses of 940 ± 720 Gy and 930 ± 170 Gy were obtained by ESE and cw-ESR, respectively.

(c) Removal of the intense signal of Mn^{2+} by electron spin echo

A cw-ESR spectrum and a field sweep ESE spectra of a manganese rich calcitic shell collected at Texas are shown in Fig. 2-11 where the interpulse time was 500 ns. Only the free induction decay (FID) of SO_3^- was detected and its

intensity was taken as an ESE intensity. No signal of Mn^{2+} was detected for ESE, while the intense signal of Mn^{2+} was superposing on the signal of SO_3^- ($g_\perp$ = 2.0038 and $g_{//}$ = 2.0023) for cw-ESR. The signal of CO_2^- was so weak that it was not detected in the sample.

Generally, some fossil calcitic samples contain Mn^{2+} which disturbs to determine the precise intensity of the dating signal such as CO_2^-. The ESE measurement is useful when the dating signal is interfered by the signal of Mn^{2+}. Selection of an intensity of a particular signal from overlapping signals can be a breakthrough in ESR dating when natural samples contain paramagnetic impurities.
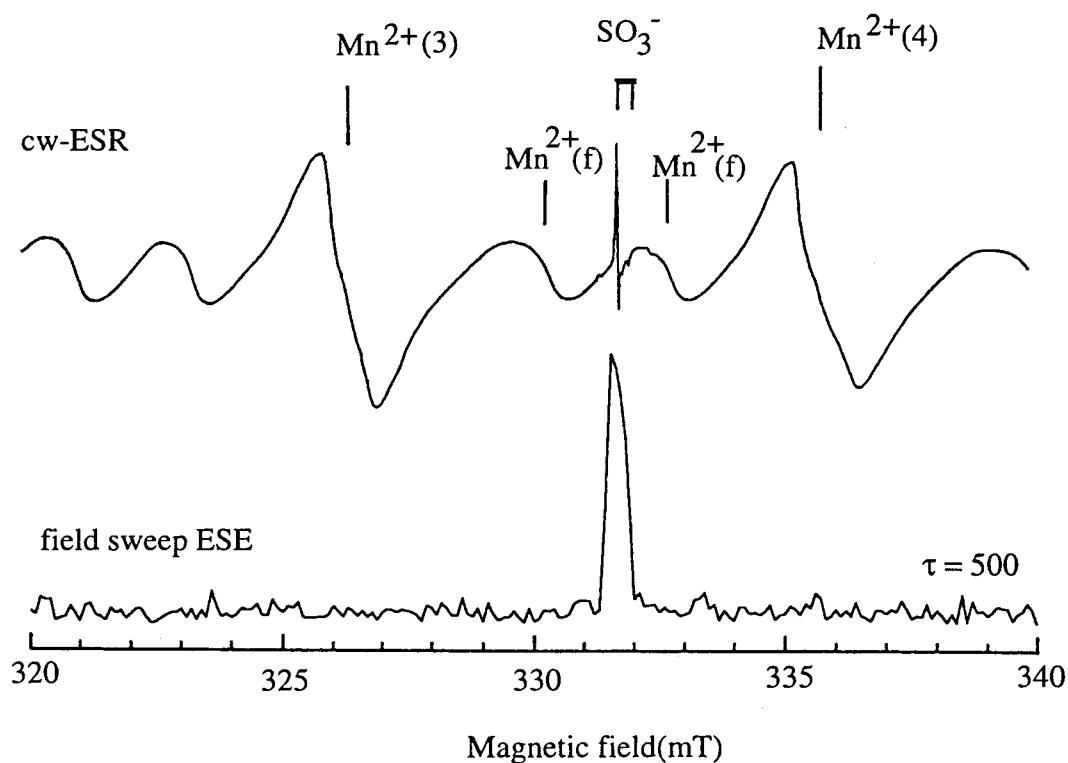

Fig. 2-11: The first-derivative cw-ESR and the field sweep ESE spectra of fossil calcitic shell collected at Texas. The intense signals of Mn^{2+} are not observed and the signal of SO_3^- is selectively detected in the ESE spectrum.

36

§3. SiO$_2$ (Quartz)

3.1 Production of E' centers and its properties

The formation mechanism of E' center in natural quartz grain is somewhat puzzling. E' centers are hardly formed in crystalline quartz by additive gamma-irradiation without preceding oxygen vacancies with paired electrons which are not paramagnetic. Gamma-irradiation does not lead to appreciable vacancy formation but alpha recoil may do (Rink and Odom, 1991). On the other hand, the formation of E' centers by mega-gray gamma-irradiation is reported (Wieser and Regulla, 1989).

E' centers are easily formed in the crushed quartz grains by additive gamma-irradiation (Toyoda *et al.*, 1993). It has been considered that the oxygen vacancies are formed by crushing along the dislocations so that E' centers can be formed. A cw-ESR and pulsed ESR study of E' centers in the crushed quartz is reported and its result is consistent with the above speculation (Ikeya *et al.*, 1992).

In this Chapter, E' center produced by external alpha-irradiation has been measured with cw and pulsed ESR. The line-shape, the saturation behavior and the phase relaxation times, T_2, have been compared with those by fast neutrons, by crushed-and-gamma-irradiation and in gamma-irradiated silica glass. The formation mechanism of E' center is discussed.

3.1.1 Experimental

Sample preparation
Sample A (alpha-ray irradiation): Quartz grains of 99.9 % in purity were crushed into powder and fraction between 75 and 106 μm was collected. Sample was annealed at 600 °C for 3.5 hours to remove the ESR signals and oxygen vacancies. The samples were irradiated by He$^+$-particles using a Van de Graaff accelerator with the energy of 1.8 MeV. The beam intensity was about 2×10^{11} particles/cm^2 and the irradiation times were about 1 s, 10 s and 100 s. The sample irradiated for 100 s was used for measurements of the line-shape, the saturation behavior

and pulsed ESR.

<u>Sample N (neutron-irradiation)</u>: The annealed quartz grains were also irradiated by 14 MeV fast neutrons to the dose of 2.4×10^{14} n/cm^2 using an Oktavian accelerator utilizing the D-T reaction by the bombardment of D$^+$ on a titanium-tritium target.

<u>Sample C (crushed fine grains)</u>: The annealed quartz grains with no ESR signals and oxygen vacancies were crushed and the fraction having diameter less than 5 μm was collected. The sample was irradiated by gamma-rays from the source of ^{60}Co with a dose of 435 Gy.

<u>Sample G (silica glass)</u>: Silica glass irradiated by gamma-rays with a dose of 18 kGy from the source of ^{60}Co.

<u>Sample V (for the Al hole center study)</u>: The annealed quartz grains irradiated by gamma-rays to produce aluminum hole centers.

ESR measurements

<u>E' center</u>: ESR measurements were done with a commercial X-band ESR spectrometer (JEOL RE-1X), where the field modulation width was 0.01 mT at a modulation frequency of 100 kHz and the microwave power was 0.01 mW at room temperature. The first-derivative spectra were measured. Pulsed ESR measurements were also performed. The dead time was about 400 ns with a microwave power of about 20 W.

<u>Al center</u>: cw-ESR measurements were performed at 77 K with a modulation width of 0.1 mT and microwave power of 5 mW.

3.1.2 Results and discussion

(a) Properties of E' center

The cw-ESR spectrum of E' centers in each sample measured at room temperature is shown in Fig. 3-1 for the sample-A, N, C and G (described in the section of experimental). The line-shape of ESR absorption of E' center in alpha-irradiated quartz is similar to that for neutron-irradiation, while the line-width is broadened compared to that for neutron-irradiation. There are two possibilities, (1) E' centers are localized along the alpha-tracks with higher

concentration than that for neutron-irradiation and (2) the irradiation flux was so high as to produce the high local concentration on the surface (about 10 μm in depth). The average spin concentration of E' centers in the sample-A was 2.5 × 10^{14} spins/g that was almost twice that of the sample-N. The local concentration of the E' centers in the sample-A must much higher than that of the sample-N. The high concentration will lead strong spin-spin interactions and broaden the absorption line-width of each spin-packet. However, it is not clear which is the main contribution.

The small Gaussian-distribution in g_2 and g_3 has been reported for E' centers in gamma-irradiated fused silica (Griscom, 1979), while the g_1 value has no distribution that leads a strong peak at g_1. Our observation is consistent with the report. E' centers in gamma-irradiated silica glass show a unique line-shape due to the distribution of g-factors.

E' centers produced by crushing followed by gamma-irradiation show a similar line-shape to that for glass and has a broader line-width. The amorphous parts would be formed by crushing along the micro cracks where E' centers are easily formed directly by additional gamma-irradiation, while E' centers are not produced in crystalline part. Excitons formed by radiation might lead to the formation of oxygen vacancies and interstitials in amorphous region: vacancies and interstitials are stabilized by the lattice distortion. Oxygen vacancies also might be created by crushing along dislocations and the following gamma-irradiation converts the oxygen vacancies to E' centers. These processes lead to the higher local concentration of E' centers along the dislocations than the average concentration of E' centers in the sample-G of 2.8 × 10^{17} spins/g, while the average concentration is 1.4 × 10^{16} spins/g for the sample-C. The observed broad line-width for crushed and gamma-irradiated quartz may be either due to the strong spin-spin interactions or to the lattice deformation.

It is interesting that E' center produced by alpha-irradiation is not 'glassy'. E' centers were produced in crystalline part. We expected that the alpha-irradiation should form the amorphous parts along the alpha-tracks and expected that E' centers produced by alpha-irradiation should be 'glassy'.
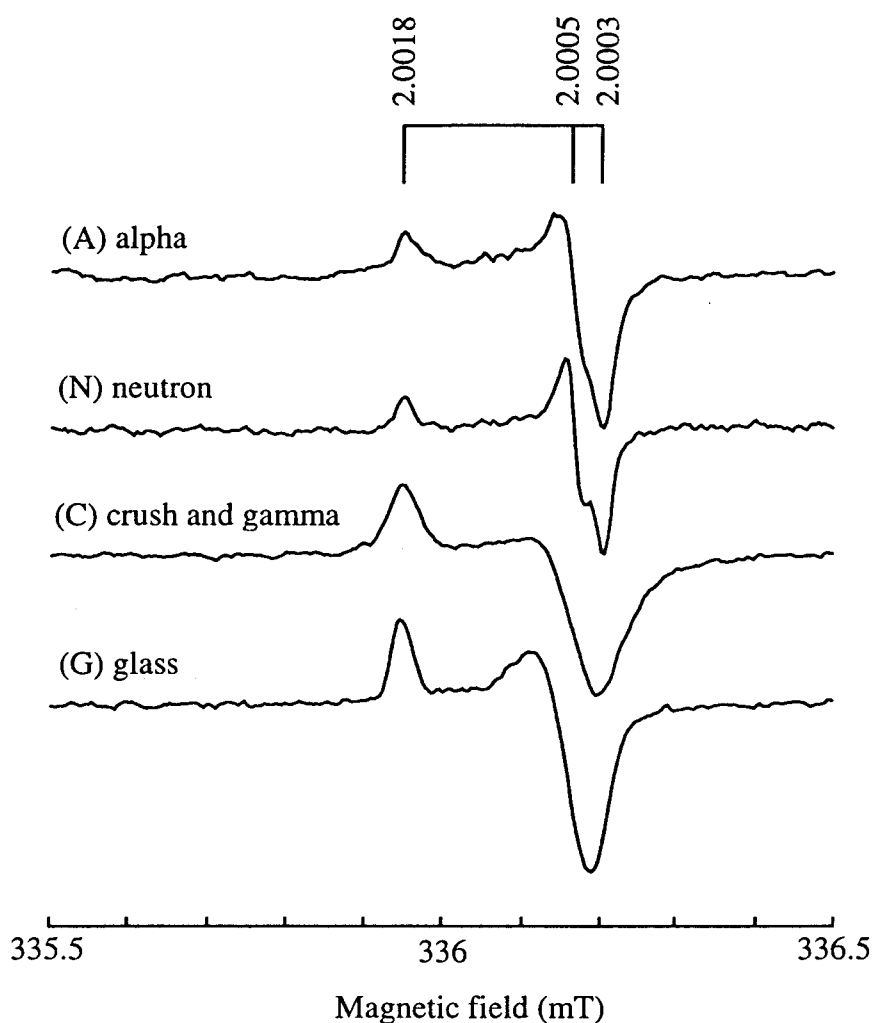
Fig. 3-1: The first-derivative cw-ESR spectra of E' centers in (A) alpha-irradiated quartz, (N) neutron-irradiated quartz, (C) crushed and gamma-irradiated quartz and (G) gamma-irradiated silica glass. Measurements were performed at room temperature at the microwave power of 0.01 mW with the 100 kHz modulation of 0.01 mT width.

Figure 3-2 shows the microwave power dependence of E' center in the sample-A, N, C and G. ESR signal of E' center in the sample-N saturates easily compared to those in the other samples. The saturation behavior of E' centers in the sample-A is similar to those of the sample-C. The slope at high microwave power for the sample-G decreases moderately.

The ratios of the line-width of the spin packet and the line-width of inhomogeneous broadening, $\Delta H_L / \Delta H_G$, were determined from the saturation curves (Castner, 1959), where the Lorentzian and the Gaussian functions were assumed for homogeneous and inhomogeneous broadening, respectively. The amplitude of the magnetic field of the microwave (H_1) is proportional to the square root of the microwave power (P) as,

$$H_1 \propto \sqrt{P} \ . \tag{3-1}$$

The amplitudes of the magnetic fields of the microwave at the half of the maximum absorption are termed as $H_1(V_{1/2lower})$ and $H_1(V_{1/2upper})$, then its ratio is obtained as,

$$\frac{H_1\left(V_{1/2\,upper}\right)}{H_1\left(V_{1/2\,lower}\right)} = \sqrt{\frac{P\left(V_{1/2\,upper}\right)}{P\left(V_{1/2\,lower}\right)}} \ . \tag{3-2}$$

The ratio, $\Delta H_L / \Delta H_G$, is obtained from the value of eq.(3-2). The obtained ratios of 0.1 (alpha), 0.09 (neutron), 0.07 (crushing) and 0.02 (glass) might involve a considerable amount of errors but the large inhomogeneity for gamma-irradiated glass is certain. It is not clear why the ESR signal of E' centers in the sample-C is not inhomogeneously broadened, though the line-shape indicates that E' are formed in glassy region.
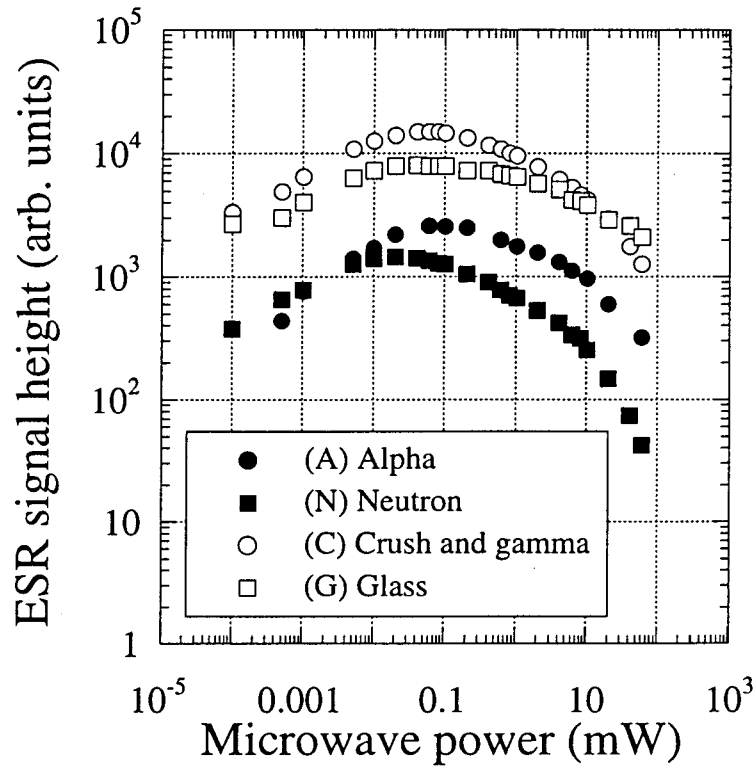
Fig. 3-2: The microwave power dependence of the ESR signal intensity of E' center in (A) alpha-irradiated quartz, (N) neutron-irradiated quartz, (C) crushed and gamma-irradiated quartz and (G) gamma-irradiated silica glass.

A typical electron spin-echo shape of E' centers in crushed sample is shown in Fig. 3-3, where the data accumulation of 6000 times for averaging was done. Figure 3-4 shows the decay curves of spin-echo intensity plotted as a function of the time interval between the first $\pi/2$ pulse and the second π pulse for the sample A, N, C and G. The spin echo intensities are normalized with the initial amplitude at $\tau = 400$ ns. The decay curve gives the phase relaxation time, T_2, from the fitting to an exponential decay curve written as follows:

$$I(\tau) = I_0 \exp(-2\tau/T_2) + (\text{noise level}) \ . \tag{3-3}$$

The obtained phase relaxation times are 6.5 ± 0.4 μs (sample-A), 15.9 ± 1.0 μs (sample-N), 7.3 ± 0.2 μs (sample-C) and 18.5 ± 0.2 μs (sample-G) (see Table 3-1). The short relaxation times for the sample-A and C should be due to strong spin-spin interactions and are consistent with their line-widths. The average concentration of E' centers in the sample-G is highest of all, however its relaxation time is longer than that for neutron irradiated quartz. The relaxation process in a glass is different from that in a crystalline quartz.
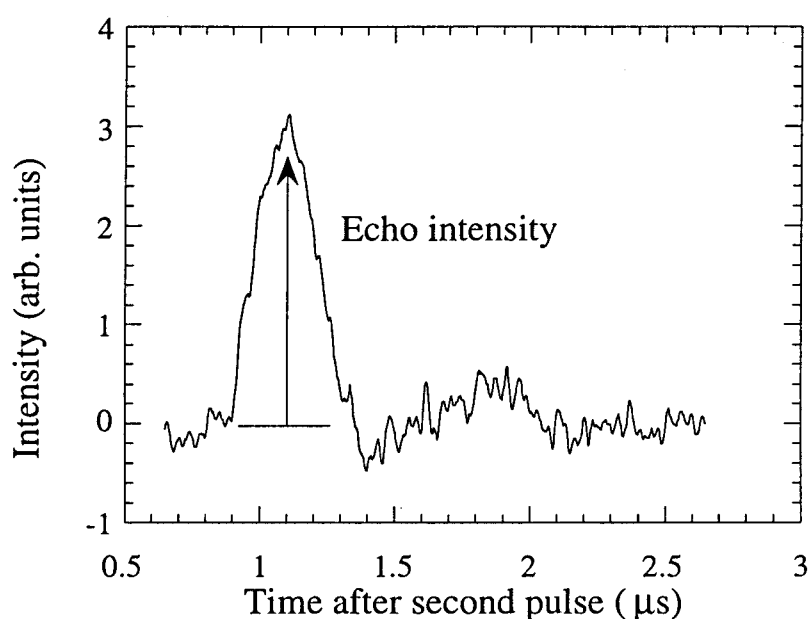

Fig. 3-3: The electron spin echo shape of E' centers in crushed quartz. Data was accumulated for 6000 times and averaged. The phase alternation was also applied.
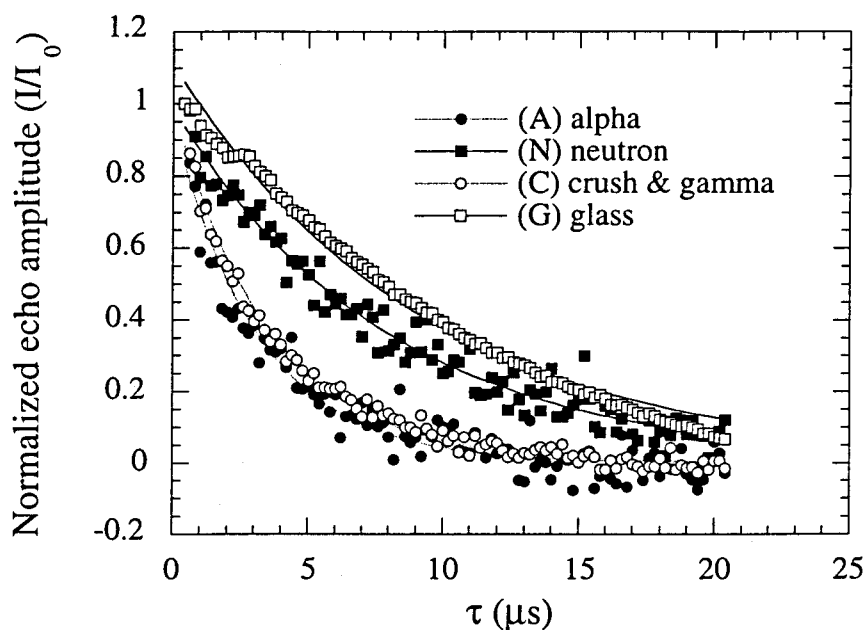
Fig. 3-4: Decay curves of spin-echo intensity plotted as a function of the time interval between π/2 pulse and π pulse.

Table 3-1: Observed E' centers in crystalline quartz and silica glass.

Samples	line shape	linewidth	$\Delta H_L/\Delta H_G$[a]	T_2 (μs)	spin density (g⁻¹)
(A) Alpha-irrad. Qz	C-type[b]	broad	0.1	6.5 ± 0.4	2.5×10^{14}
(N) Neutron-irrad. Qz	C-type	narrow	0.09	15.9 ± 1.0	1.3×10^{14}
(C) Crushed and gamma-irrad. Qz	A-type[c]	broad	0.07	7.3 ± 0.2	1.4×10^{16}
(G) Gamma-irrad. silica glass	A-type	narrow	0.02	18.5 ± 0.2	2.8×10^{17}

a) The estimated ratio of the homogeneous broadening and the inhomogeneous broadening.
b) Crystalline type.
c) Amorphous type. The g_2 and g_3 factors of amorphous-type E' center are distributed with gaussian function.

(b) Dose and grain size dependence of T_2 of E' centers in crushed and gamma-rayed quartz

The crushed quarter was sieved into several ranges and irradiated by gamma-rays to several doses. The obtained T_2's were tabulated in Table 3-2 and were plotted in Fig. 3-5. The intensity of spin echo was too weak to detect for some samples. The T_2 decreases as the dose increases because the concentration of E' center is increased by gamma-irradiation leading to the strong spin-spin interaction. The T_2 for large grain size is shorter than that for small grain size except for the datum for the dose of 7.93 kGy and the grain size of 30 ~ 38 μm .
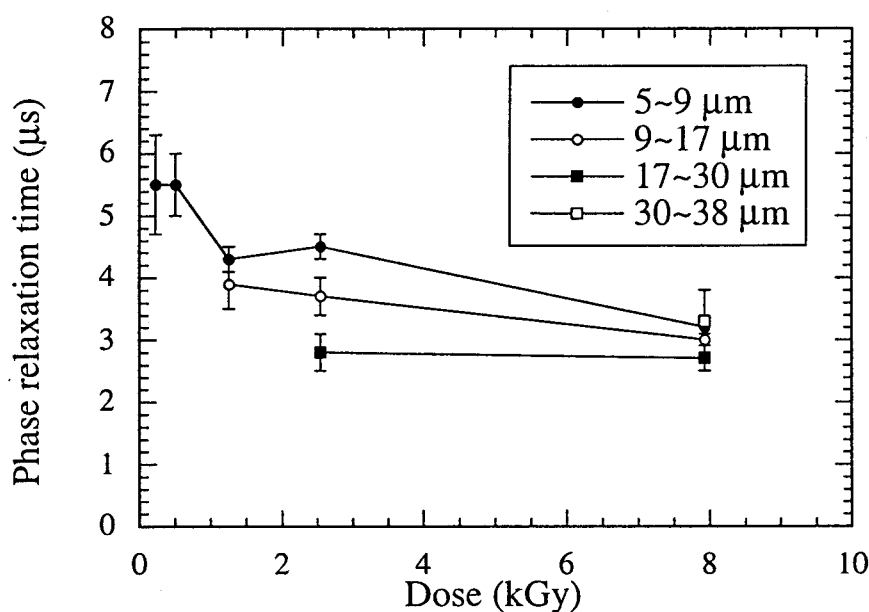
Fig. 3-5: Dose and grain size dependence of T_2 of E' centers in crushed and gamma-rayed quartz.

Table 3-2: Phase relaxation times, T_2 of E' centers in crushed and gamma-irradiated quartz.

Grain size (μm)	T_2 (μs) at 225 Gy	509 Gy	1.27 kGy	2.55 kGy	7.93 kGy
5 ~ 9	5.5 ± 0.8	5.5 ± 0.5	4.3 ± 0.2	4.5 ± 0.2	3.2 ± 0.1
9 ~ 17	-	-	3.9 ± 0.4	3.7 ± 0.3	3.0 ± 0.2
17 ~ 30	-	-	-	2.8 ± 0.3	2.7 ± 0.2
30 ~ 38	-	-	-	-	3.3 ± 0.5

(c) Alpha efficiency in producing E' centers and aluminum centers

Amount of defects produced by alpha-irradiation are plotted as a function of absorbed dose for E' center and aluminum center (a hole at an aluminum atom) in Fig. 3-6(a). The production efficiency per 100 eV of alpha-particles, G value, are about 10^{-4} and 10^{-2} per 100 eV for E' center and aluminum center, respectively. The $G = 10^{-4}$ corresponds to only one defect per 1.8 MeV alpha particle. One E' center is produced along an alpha track. The strong spin-spin interaction for alpha-irradiated quartz must be due to the high local concentration of defects in the irradiated surface volume with the depth of about 10 μm caused by high dose to obtain a sufficient signal intensity.

The relative alpha efficiency against gamma-irradiation (see Fig. 3-6(b)), k-value, of 0.012 for aluminum center for 1.8 MeV was obtained from the parameters of the curve fittings.
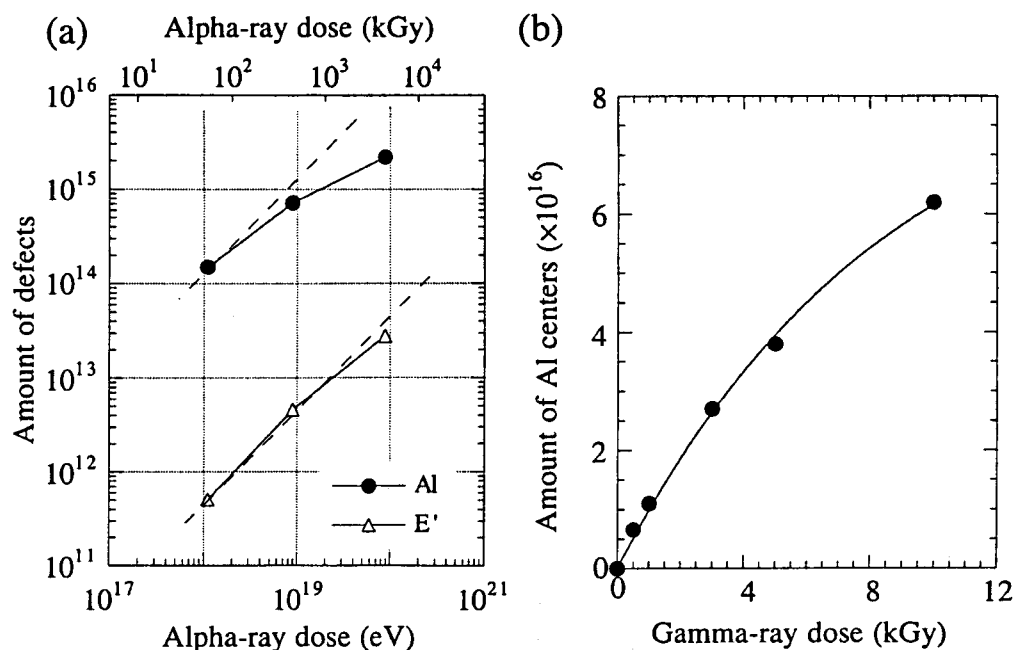
Fig. 3-6: (a) Amount of defects produced by alpha-irradiation with varying the radiation dose for E' center and Al centers. (b) Growth curve of Al centers by gamma-irradiation.

(d) Implication for ESR dating

Results are summarized in Table 3-1. The shape of E' produced by outer alpha-irradiation is very similar to that in natural quartz. It may be difficult to distinguish the effects of outer alpha-irradiation from neutron-irradiation (and mega-rad gamma-irradiation) in producing E' centers in quartz. On the other hand, 'glassy' shape of E' center in crushed and gamma-irradiated quartz and its short spin-spin relaxation time, T_2, should be useful for signal separation. The 'glassy' signal may be formed at the time of fault movement and enhanced by additive natural radiation. Zeroing of signal at a fault movement is not necessary for the dating of fault movements if the signal of E' centers in the 'glassy' parts is detected in the quartz in the fault gouge.

3.2 ESR dating of Rokko fault by signal separation

ESR signal of E' centers in quartz extracted from granite has a sharp linewidth and its line-shape is crystalline-type, while that in crushed and gamma-irradiated quartz has a broad linewidth and has an amorphous-type line-shape. A part of E' centers in granitic quartz may annealed mechanically and thermally when a fault moved. Following natural radiations can hardly produce E' centers in crystalline part of quartz. On the other hand, amorphous region may formed by crushing where a lot of oxygen vacancies exist and E' centers are easily produced by additive gamma-irradiation. It is expected that two types of E' centers exist in quartz collected from fault gouge; one is the "crystalline-type" one and another is the "amorphous-type" one which is unique to crushing.

3.2.1 Experimental

The cw-ESR spectra of E' centers in granitic quartz, in crushed and gamma-irradiated quartz and in fault gouge collected at Rokko, Japan were recorded numerically using a personal computer. ESR measurements were made with a commercial X-band spectrometer at room temperature, where a microwave power was 0.01 mW and a magnetic field modulation width was 0.0125 mT with a frequency of 100 kHz. It was assumed that ESR signal of E' centers in fault gouge, f_i is a linear combination of ESR signals of E' centers in granitic quartz, g_i and in crushed and gamma-irradiated quartz, h_i;

$$f_i = a\,g_i + b\,h_i ,\qquad(3\text{-}4)$$

Each component was determined by the least square method.

Two samples were collected from the main fault zone of Rokko fault, Japan. The distance between two sampling sites is about 1.5 m. Samples were sieved and the fraction under 38 μm was collected and dried at 50 °C for two days to remove water before ESR measurements.

3.2.2 Results and discussion

Figure 3-7 shows the signal enhancements of two components by the additive gamma-irradiation for two samples. The component of the "crystalline-type" does not be enhanced by gamma-irradiation. This result is consistent with the report that E' centers hardly produced by gamma-irradiation without oxygen vacancies these are precursor of E' centers (Garrison et al., 1981).
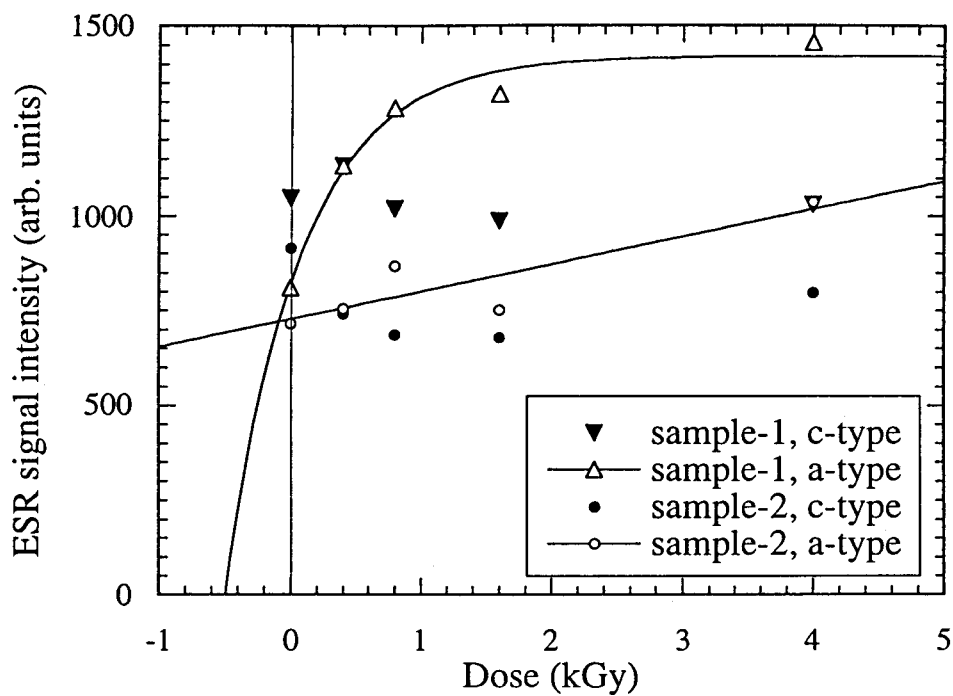

Fig. 3-7: ESR intensities of E' centers plotted as a function of gamma dose. The "c-type" and the "a-type" correspond to the crystalline-type and the amorphous-type. The age of fault movement is obtained using ESR signal of "a-type" E' centers.

On the other hand, the component of the "amorphous-type" E' centers produced by crushing and following gamma-irradiation is enhanced by additive gamma-irradiation because E' centers are easily produced in the amorphous region. Data were fitted to a saturation growth curve and total doses of 0.5 ± 0.1 kGy and 10 ± 4 kGy were obtained. The obtained total doses correspond to the

age of 69 ± 14 ka and 1.4 ± 0.5 Ma using as annual dose rate of 7.2 mGy obtained by thermoluminescence dosimeter (TLD). Ikeya, 1993 estimated the age of Rokko fault as 150 ~ 180 ka assuming the zeroing of E' centers by crushing and heating at the fault movement. The reported age may be overestimated because of the partial zeroing of E' centers. It can be concluded that the age of 69 ± 14 ka may be more reliable than others.

§4. Evaporites

Secondary mineral deposits precipitated or crystallized by evaporation of aqueous solution are called evaporites. The precipitation age and impurity center of evaporites are important for the study of sedimentary history and paleo-environment. ESR dating method has been used for the study of fossil shells, quartz, phosphates and evaporites by detecting the accumulated radiation dose from the concentration of the radiation-induced defects that have been accumulated in a geologic time scale. $NaHCO_3$ (nahcolite) is one of common evaporites and a few studies of ESR dating are reported (Ikeya and Kai, 1988).

In the previous studies of ESR dating, it has been assumed that the alpha-irradiation induces the same kind of defects/radicals as the gamma-irradiation except for calcium carbonate. The production efficiency of the alpha-irradiation is generally smaller than that of gamma-irradiation. The alpha-ray efficiency relative to gamma-ray, k-value, has been determined for calcium carbonate (see Chapter 2), but no study has been done for evaporates. In addition to above, no study of these evaporate minerals using pulsed ESR has been done.

4.1. Experimental

Powdered samples of the reagent-grade and natural nahcolite ($NaHCO_3$), gypsum ($CaSO_4 \cdot 2H_2O$) and barite ($BaSO_4$) were irradiated by gamma-rays from the source of ^{60}Co at the rate of about 100 Gy/h. He^+-particles irradiation was done using the Van de Graaff accelerator to study the effects of the alpha-irradiation, where the beam current was approximately 100 nA with the energy of 1.6 MeV.

Continuous wave ESR (cw-ESR) measurements were performed with the X-band ESR spectrometer (JEOL, RE-1X) at the microwave power of 1 mW and 5 mW. The 100 kHz field modulation width was 0.1 mT. Pulsed ESR measurements at the X-band frequency were also done, where the Hahn's spin-echo method was applied.

4.1.2 Results and Discussion

NaHCO₃ (nahcolite)

(a) Observed cw-ESR signals

HCO₃

Figure 4-1 shows the ESR spectra of a) gamma-irradiated and b) He^+-irradiated powdered nahcolite measured at the microwave power of 1 mW at room temperature. Six parts of ESR spectra are termed from A to F as shown in Fig. 4-1.

Fig. 4-1: The first derivative cw-ESR spectra of a) gamma-irradiated $NaHCO_3$ and b) alpha-irradiated $NaHCO_3$. HCO_2 (or CO_2^-, the dip at $g = 1.997$) were produced by both gamma- and alpha-irradiation. Signals are termed from A to F.

Intensities of the signal A to F were plotted as a function of the applied microwave power in Fig. 4-2 to identify the ESR signals. The intensities increase proportionally to the square root of the microwave power up to about 10 mW but a pair of A and B and a pair of C and F saturate similarly; therefore, these signals should be due to the same defect.

The signals A and B has a characteristic powder spectrum of defect with an orthorhombic symmetry. The orthorhombic signal has the g-factors of 2.021, 2.007 and 2.004 similar to those of HCO_3 ($g_1 = 2.0184$, $g_2 = 2.0087$ and $g_3 = 2.0059$) in $KHCO_3$ (Holmberg, 1971). The reported splitting by a proton was about 0.2 mT and was not resolved even in the single crystal study. Hence, no doublet by a proton is expected in the powdered spectrum. That is consistent with our observation in $NaHCO_3$. The hyperfine splitting by a proton only broadens the linewidth as the splitting by the magnetic moment of Na^+.

HCO_2 or CO_2^-

The signal-C (the dip at $g = 1.997$) in gamma-irradiated nahcolite and the signal-F in He^+-irradiated nahcolite should be HCO_2 or CO_2^- as assigned by Holmberg, 1971. The radical could not be unambiguously ascribed as a proton hyperfine interaction although the possibility that the radical contains hydrogens could not be excluded. The signal intensity of this radical is maximum at the microwave power of about 4 mW and slightly decrease at higher microwave power.

$(HCO_3)_2^-$

The signals E and D behave similarly up to 40 mW but independently at a high microwave power. The difference would be due to the noise on the signal D. Signal D and E may be related with an axial signal with $g_{//} = 2.028\text{-}9$ and $g_\perp = 2.007\text{-}8$. Comparing with the reported g-factors for radiation induced defects in $KHCO_3$, this signal may be ascribed to $(HCO_3)_2^-$ ($g_1 = 2.0261$, $g_2 = 2.0079$ and $g_3 = 2.0063$ in $KHCO_3$). The obtained linewidth of the signal D at half the maximum intensity was $0.4 \sim 0.5$ mT that is in good agreement with the hyperfine coupling constant of $0.28 \sim 0.46$ mT by two equivalent protons reported for $(HCO_3)_2^-$ in $KHCO_3$. The hyperfine interaction with protons may broaden the

linewidth of the powdered spectrum so that the orthorhombic symmetry of this radical may change to axial symmetry because of the small difference between g_2 and g_3.
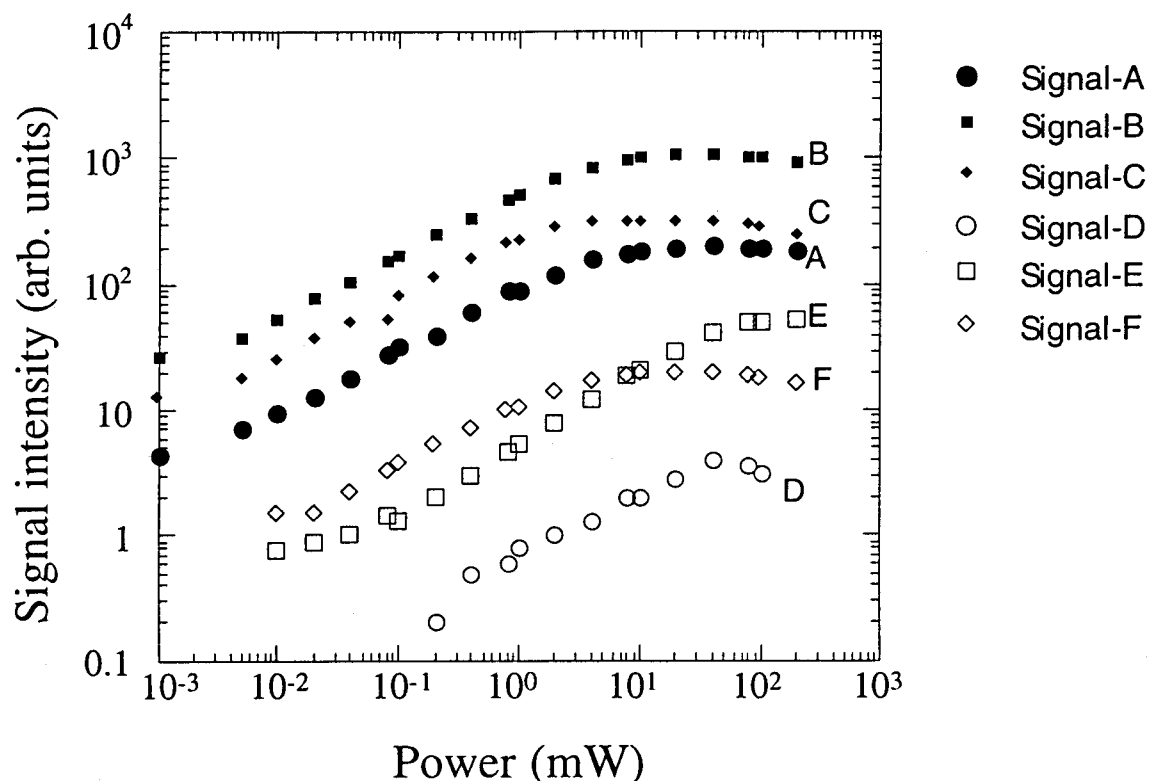

Fig. 4-2: The microwave power dependence of the ESR signals A to F.

(b) Alpha-ray defect production efficiency for HCO_2 (or CO_2^-)

In this study, the relative dip height at $g = 1.997$ was used as a signal intensity to determine the k-value for HCO_2 (or CO_2^-) because the line width and the g-factor were same for both gamma- and alpha-irradiations. That assures the linearity in the addition of the peak heights.

Figure 4-3 shows the signal intensity of HCO_2 (or CO_2^-) plotted as a function

of the absorbed dose. The absorption dose for gamma-irradiation was the energy absorbed in a sample of 100 mg. The k-value of 0.085 for HCO_2 at $g = 1.997$ was obtained for 1.6 MeV He^+-irradiation from the fitting parameters of growth curves. An effective k-value of 0.11 in equilibrium of ^{238}U-series for ESR dating was obtained.

We need not consider the alpha-dose when the HCO_3 is used as a dating signal because the HCO_3 is not produced by the alpha-irradiation. Similarly, the use of $(HCO_3)_2^-$ requires only alpha-dose, while the use of HCO_2 (or CO_2^-) needs alpha, beta and gamma doses. This indicates that three equivalent doses are obtained from one sample by additive dose method. This may be useful for the cross checking of ESR age and may lead to more precise ESR dating and dosimetry.
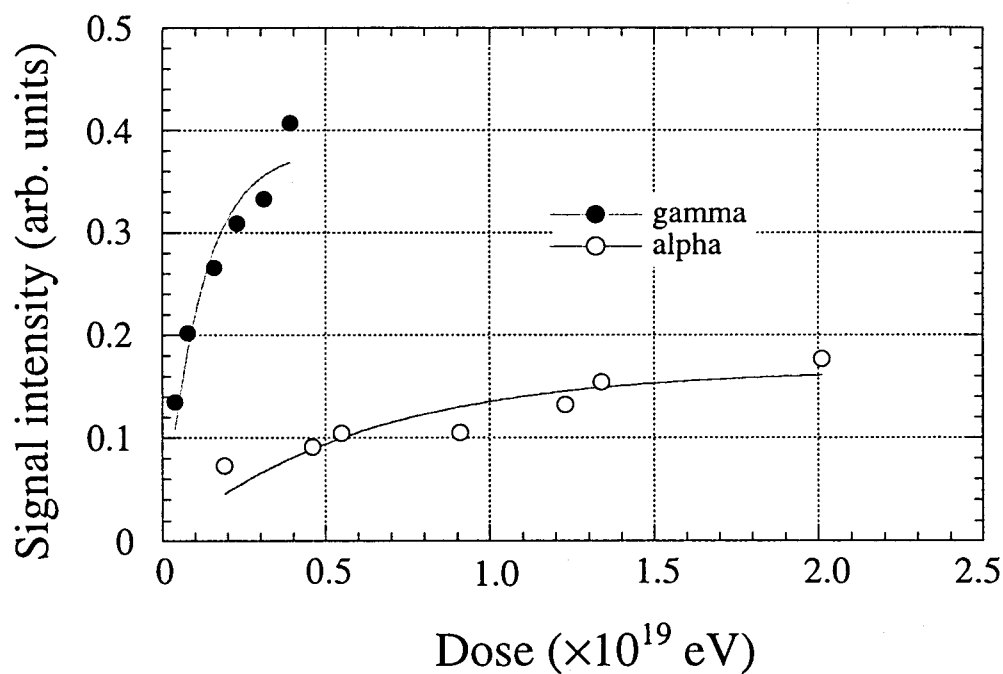

Fig. 4-3: The signal intensities of HCO_2 (or CO_2^-) plotted as a function of the absorbed doses for both gamma- and alpha-irradiations.

55

(c) Pulsed-ESR measurements

The field sweep electron spin echo (ESE) spectra of gamma-irradiated nahcolite at τ = 400 ns (solid line) and 800 ns (dotted line) were shown in Fig. 4-4, where the τ is the time interval between the first $\pi/2$-pulse and the second π-pulse. The peak at 330.7 mT due to HCO_3 had been already decayed at the pulse interval of 800 ns, while that of HCO_2 (or CO_2^-, peak at 331.5 mT) was observed at both τ = 400 ns and 800 ns with no decay. The selective measurement of HCO_2 (or CO_2^-) from overlapped signals is possible by pulsed ESR with a sufficient long τ.
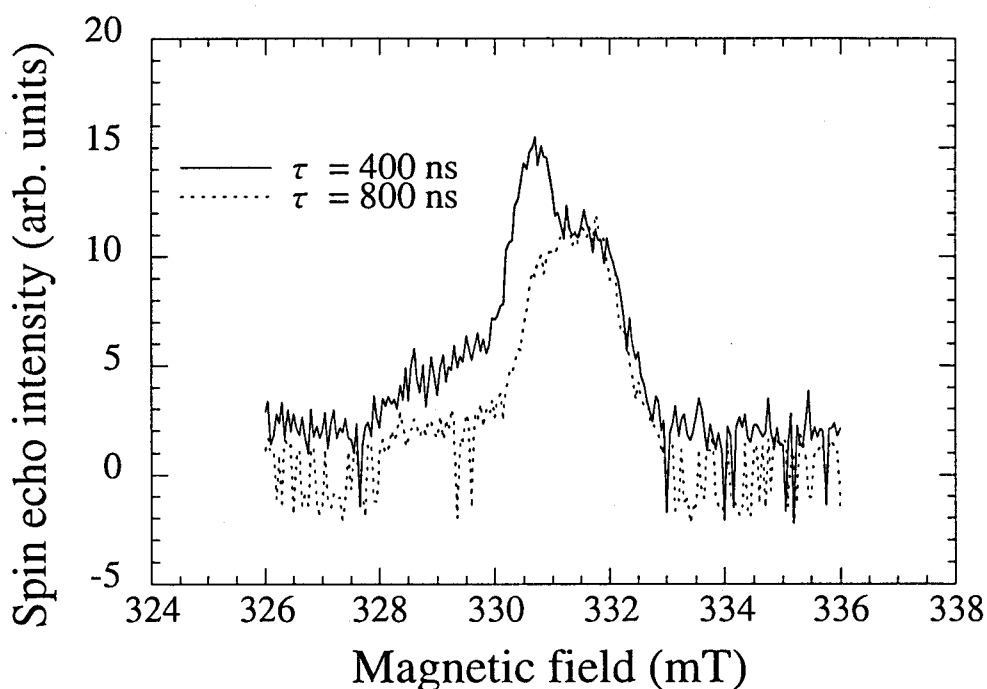

Fig. 4-4: The field sweep ESE spectra of $NaHCO_3$ irradiated by gamma-rays with the dose of 40 kGy with pulse intervals, τ, of 400 ns and 800 ns. The signal of HCO_3 has decayed at τ = 800 ns.

Figure 4-5 shows the echo amplitudes plotted as the function of the pulse interval, τ, for both (a) HCO_2 (or CO_2^-) and (b) HCO_3. The echo of HCO_3 decays faster than that of HCO_2 (or CO_2^-) and that is consistent with the result of field sweep ESE measurements. The obtained phase relaxation times, T_2, were 2.3 ~ 2.7 μs for HCO_2 and 0.8 ~ 1.1 μs for HCO_3.
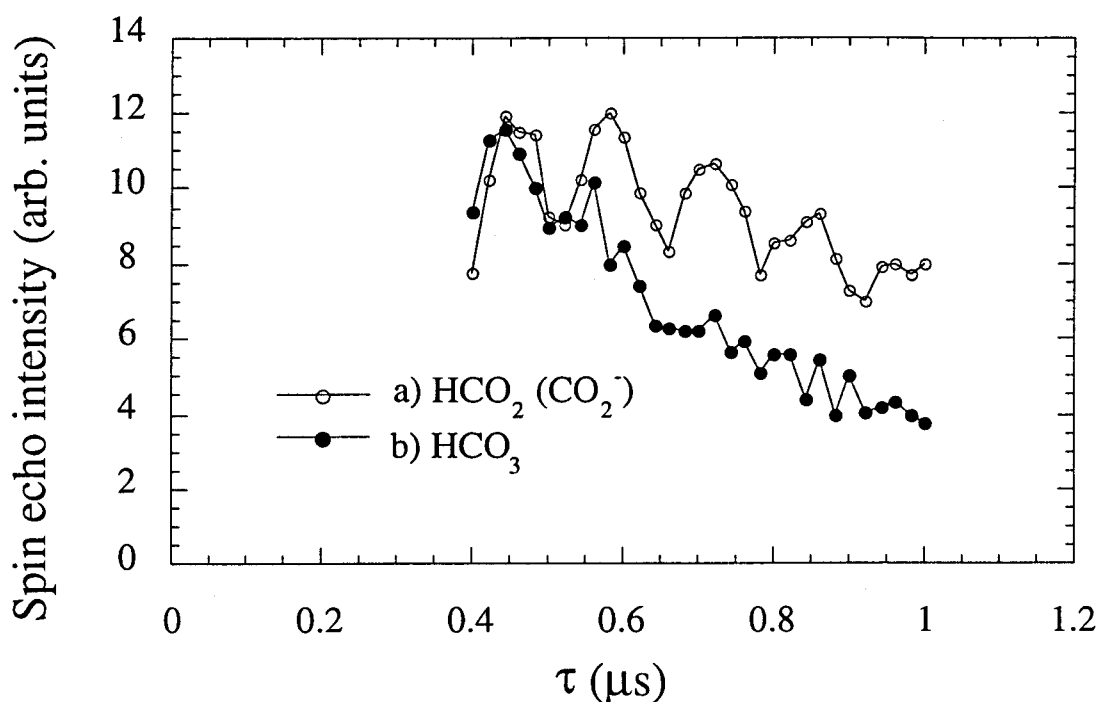

Fig. 4-5: The decays of the spin echo intensities of a) HCO_2 (or CO_2^-) and b) HCO_3 measured at room temperature for gamma-irradiated $NaHCO_3$. The decay for HCO_2 (or CO_2^-) is modulated with the frequency of 7 ~ 8 MHz and slower than that for HCO_3. The obtained phase relaxation times are 2.3 ~ 2.7 μs and 0.8 ~ 1.1 μs for HCO_2 (or CO_2^-) and HCO_3, respectively.

The spin echo envelope of HCO_2 (or CO_2^-) was modulated with the frequency of 7.5 ± 0.5 MHz that is about twice the Larmor frequency of Na nucleus (3.7 MHz at 331 mT, $I = 3/2$, 100 % in abundance), while no clear modulation was observed for HCO_3. Spin-echo often has a periodic intensity variation which is

caused by weak nuclear hyperfine interactions and called electron spin echo envelope modulation (ESEEM) (Rowan *et al.*, 1965). The double frequency has been predicted in the simulation study of ESEEM (Dikanov, 1981).

The modulation amplitude, V_{mod}, is expressed with some approximations for powdered spectrum as

$$V_{mod} = \left[\frac{1}{2} \int_0^\pi V(\tau, \theta) \sin\theta d\theta \right]^n$$

$$V(\tau,\theta) = V(0,\theta) \left[1 - \frac{8}{3} I(I+1) \left(\frac{B\omega_n}{K^+ K^-} \right)^2 \sin^2\left(\frac{K^+ \tau}{2} \right) \sin^2\left(\frac{K^- \tau}{2} \right) \right]$$

$$K^\pm = \left[\left(AS_z \pm \omega_n \right)^2 + \left(BS_z \right)^2 \right]^{1/2} \qquad \text{, (4-1)}$$

$$A = \frac{1}{\hbar} \left\{ \frac{g g_n \beta \beta_n}{r^3} \left(3\cos^2\theta - 1 \right) + 2\pi\alpha \right\}$$

$$B = \frac{1}{\hbar} \frac{g g_n \beta \beta_n}{r^3} \cdot 3\sin\theta\cos\theta.$$

where n is a number of nuclei with magnetic moment at nearest neighbor, ω_n is a larmor frequency of nuclear magnetic moment, α is an isotropic hyper-fine coupling constant in Hz and r is a distance between an electron spin and a nuclear spin.

The numerical calculation of the modulation amplitude was performed using above formula-(4-1) to simulate the effect of the isotropic hyperfine interaction on the modulation amplitude. The calculated modulation amplitude without exponential decay is shown in Fig. 4-6 with varying the hyperfine constant, a, from 10 to 16 MHz. The modulation amplitude decreases as the hyperfine constant increases. The ESEEM on the decay curve of HCO_3 signal may be weakened by the large isotropic hyperfine interaction with neighbor Na^+ ions.
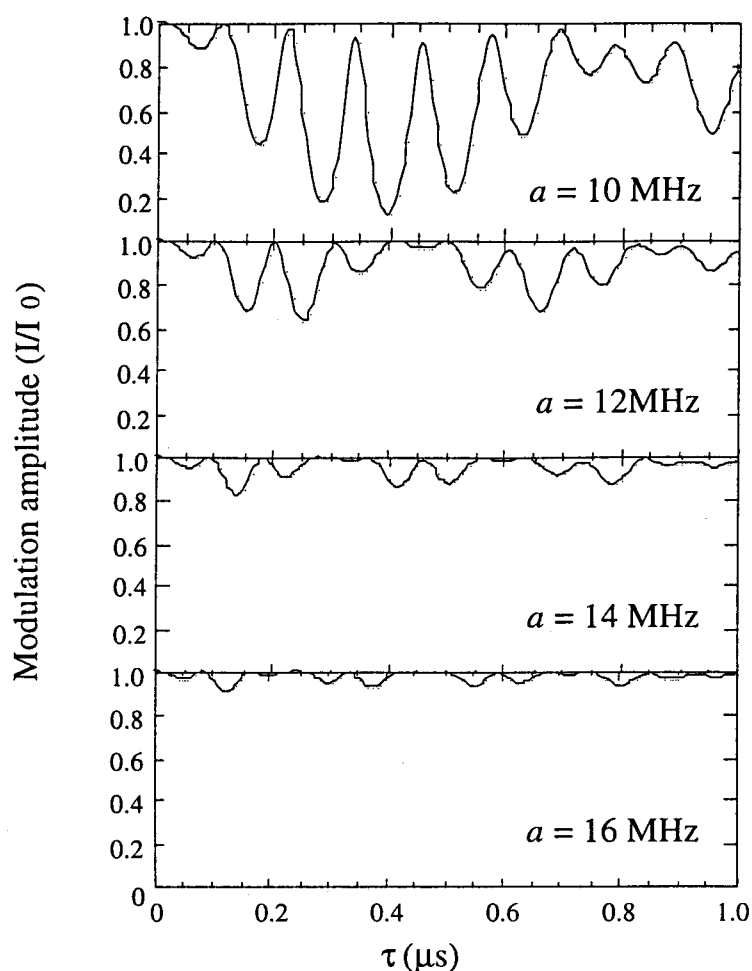
Fig. 4-6: The calculated ESEEM amplitude by Na nuclei. The isotropic hyperfine coupling constant is varied from 10 to 16 MHz. The modulation amplitude decrease as the coupling constant increases.

(d) Dating using spin echo

A natural nahcolite sample collected at Searles Lake, south California was dated using both ordinary cw-ESR and pulsed ESR method. The cw-ESR spectra of a non-irradiated sample and a sample irradiated at 1.19 kGy were shown in
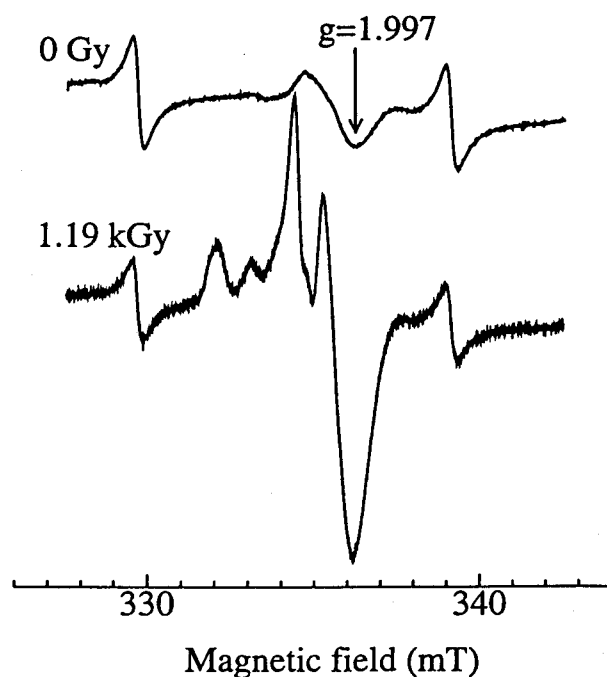
Fig. 4-7.

Fig. 4-7: The first derivative cw-ESR spectra of natural nahcolite collected at Searles Lake for non-irradiated and irradiated (1.19 kGy) sample.

Signal intensities of HCO_2 (or CO_2^-) as a function of the additive gamma dose were plotted in Fig. 4-8. The depth of the dip at $g = 1.997$ was used for the signal intensity of cw-ESR absorption and the spin echo intensity was measured at $\tau = 800$ ns where only the echo of HCO_2 (or CO_2^-) was selectively detected. The obtained data were fitted with a following function,

$$I = I_\infty\left(1 - \exp(-a(D + TD))\right), \qquad (4\text{-}2)$$

where I is a signal intensity, a is a production efficiency, I_∞ is a saturation value, D is the additive gamma dose and TD is a total dose.

The obtained total doses are 4.7 ± 4.4 kGy and 0.72 ± 0.44 kGy for spin echo method and cw-ESR method, respectively. They correspond to 9.4 ± 8.8

Ma and 1.4 ± 0.9 Ma assuming an annual dose of 0.5 mGy/a. The experimental error of the total dose obtained by spin echo was not small due to the poor S/N ratio but the obtained ages by two methods were consistent.
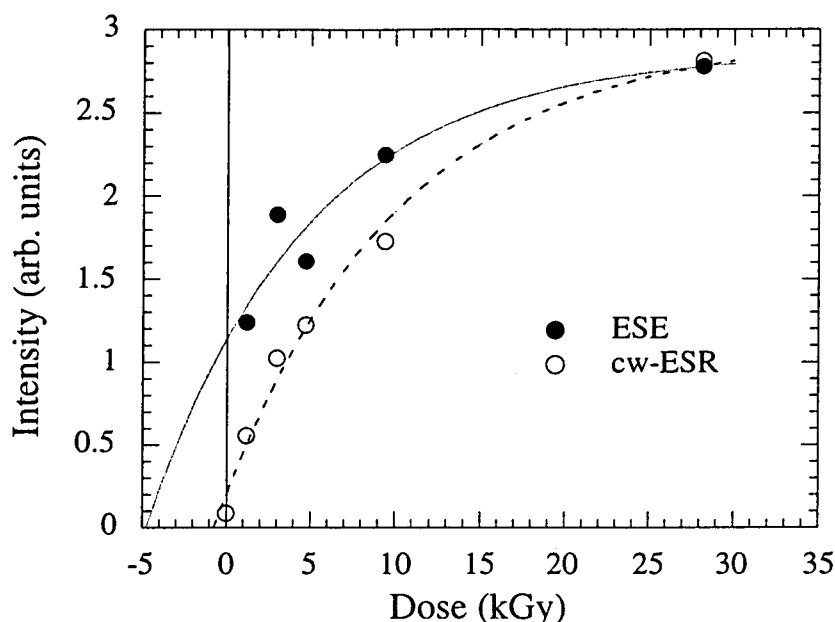

Fig. 4-8: The signal intensities of HCO_2 (or CO_2^-) measured by pulsed ESR and cw-ESR as a function of the additive dose.

(e) Summary on nahcolite ($NaHCO_3$)

Following results have been obtained from the present study.

(1) The charged particle irradiation produces HCO_2 (or CO_2^-) and $(HCO_3)_2^-$ while gamma-irradiation produces HCO_2 (or CO_2^-) and HCO_3 in $NaHCO_3$.

(2) The alpha effectiveness, k-value, of 0.11 for HCO_2 was obtained from the fitting parameters of growth curves.

(3) Pulsed ESR measurements were performed to separate the signals of HCO_2 (or CO_2^-) with $T_2 = 2.3 \sim 2.7$ μs (at room temperature) from a spectrum mixed with that of HCO_3 with $T_2 = 0.8 \sim 1.1$ μs using the different phase relaxation times.

(4) The ESEEM on a decay curve of the HCO_2 (or CO_2^-) radicals is due to neighbor Na^+ ions. The expected ESEEM by a proton was not observed in this study.

(5) ESE dating method gives the age consistent with that obtained by the ordinary cw-ESR method.

CaSO$_4$·2H$_2$O (gypsum)

Figure 4-9 shows cw-ESR spectra of synthetic powdered gypsum for (a) He$^+$-irradiation at 1.03×10^{20} eV, (b) gamma-irradiation at 40 kGy and (c) a field sweep electron spin echo (ESE) spectrum of the gamma-irradiated sample. The ESE spectrum was measured with pulse widths of 150 ns and 300 ns. The interpulse time was 500 ns. A signal of CO$_2^-$ (a dip at $g = 1.998$) and a broad signal at $g = 2.004$ were observed only in the cw-ESR spectrum of gamma-irradiated sample while a sharp signal with an isotropic g-factor of 2.003 was observed for both He$^+$ and gamma-irradiation. Some hole-type centers (CO$_3^-$ or O$_2^{3-}$) were also detected as indicated in the figure.

a) He$^+$-irradiation/cw-ESR

CO$_2^-$
2.003 1.998

b) γ-irradiation/cw-ESR

c) γ-irradiation/ESE

SO$_3^-$
2.004

330   331   332   333   334   335
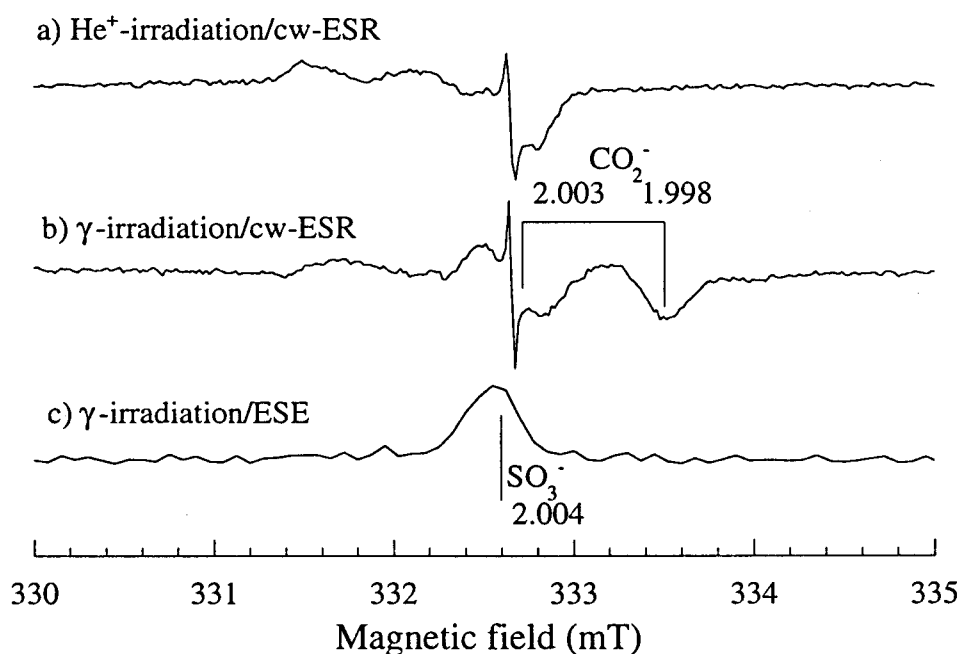Magnetic field (mT)

Fig. 4-9: The cw-ESR spectra of synthetic powdered gypsum for (a) He$^+$-irradiation at 1.03×10^{20} eV, (b) gamma-irradiation at 40 kGy and (c) a field sweep electron spin echo (ESE) spectrum of gamma-irradiated sample. Receiver gain was same for spectrum (a) and (b). No echo was detected for He$^+$-irradiated sample.

Kasuya *et al.*, 1991a reported a nearly isotropic single line at $g = 2.0028$-2.0042 in a single crystal of natural gypsum and the signal was identified as SO_3^- from hyperfine line due to ^{33}S. The distribution of the g-factor of this signal should broaden the signal for powdered sample. The broad signal at $g = 2.004$ in gamma-irradiated gypsum can be identified as SO_3^-. The sharp signal at $g = 2.004$ is not certain. A broad signal was observed in the field sweep ESE spectrum of gamma-irradiated sample, while no echo was detected for He^+-irradiated sample which has almost the same signal intensity in the cw-ESR spectrum. An echo also should be observed for He^+-irradiated sample if the echo is due to the sharp signal at $g = 2.004$; the echo may be due to the broad one (SO_3^-) in cw-ESR spectrum. Phase memory time, T_2, of 4.9 ± 0.5 μs at room temperature for SO_3^- in gamma-irradiated (40 kGy) synthetic gypsum was determined from the exponential decay of the echo (Fig. 4-10).
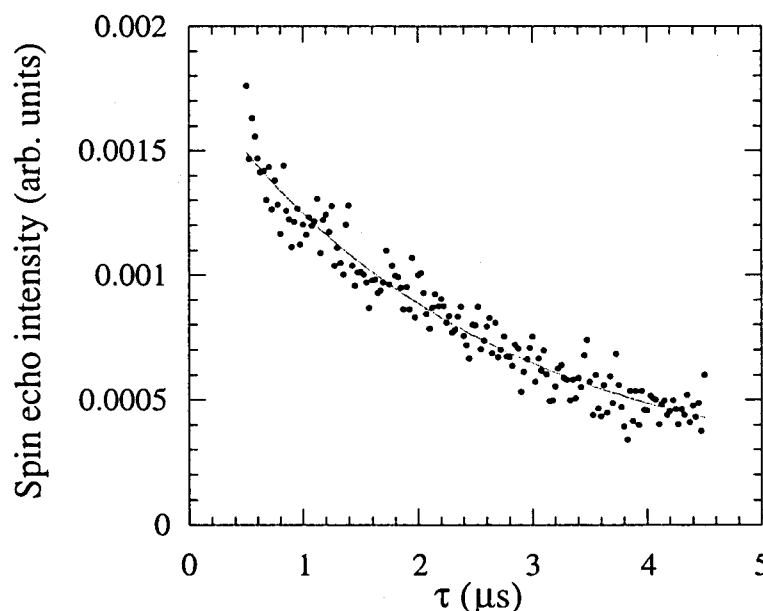

Fig. 4-10: The decay of electron spin echo of SO_3^- in gamma-irradiated synthetic gypsum measured at room temperature. The phase relaxation time, T_2, of 4.9 ± 0.5 μs was obtained.

Figure 4-11 shows the growth curves of defects in He^+-irradiated and gamma-irradiated synthetic gypsum. The entire measured spectra were doubly integrated to obtain the number of defects, no specific signal was selected. An alpha/gamma effectiveness ratio in producing defects, k-value, was determined to be 0.50 ± 0.08 for 1.6 MeV He^+ particle according to the procedure described in Chapter 2. Production efficiencies G-values were 0.0039 and 0.0078 radicals per 100 eV for He^+-irradiation and gamma-irradiation, respectively. The obtained k-value is modified to 0.66 ± 0.11 according to Lyons, 1989 for natural alpha rays considering the energy distribution of alpha-particles in radiation equilibrium.

The k-value is zero when the signals of CO_2^- or SO_3^- is used as a dating signal because hardly any of the radicals are produced by alpha-irradiation. The signal of CO_2^- is useful for cw-ESR method since it is not overlapped by others and SO_3^- is adequate for a dating signal for ESE dating method because only the signal is observed in ESE spectrum at room temperature.
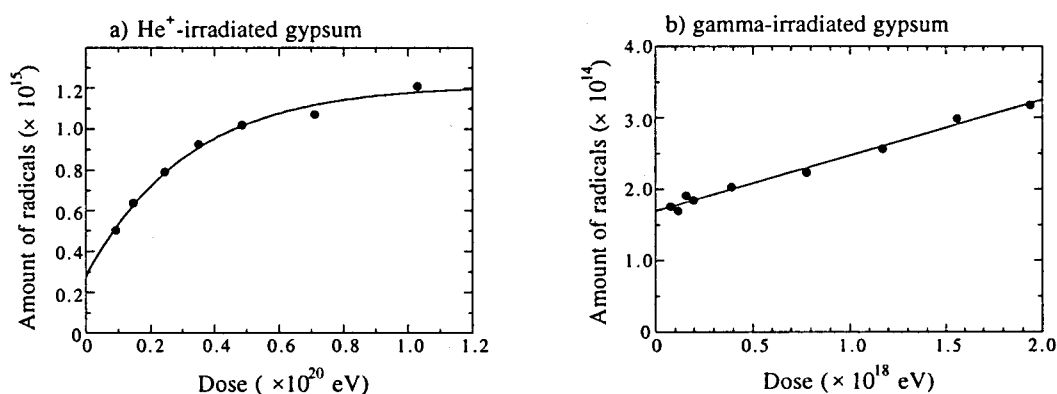

Fig. 4-11: The growth curves of defects in He^+-irradiated and gamma-irradiated synthetic gypsum. Mass of the gamma-irradiated sample is 50 mg and the area irradiated by He^+ beam is about 30 mm^2.

BaSO$_4$ (barite)

Figure 4-12 shows the cw-ESR spectra of He$^+$-irradiated and gamma-irradiated synthetic barite. The signal of SO$_3^-$ (g = 2.003, 2.002 and 1.999-2.000; reported g-factors are 2.0031, 2.0024 and 1.9995 by Ryabov *et al.*, 1983) was observed in both samples, while reported hole-type center (O$_2^{3-}$, g = 2.0191, 2.0127 and 2.0103 by Kasuya *et al.*, 1991b) was not detected. A barite rose collected from the United States which was irradiated by gamma-rays shows the ESR signal of the hole-type center as shown in Fig. 4-13. The concentration of a M^{3+} ion such as Y^{3+} which works as a stabilizer (Bershov *et al.*, 1971) in synthetic barite may be different from that in natural barite rose.
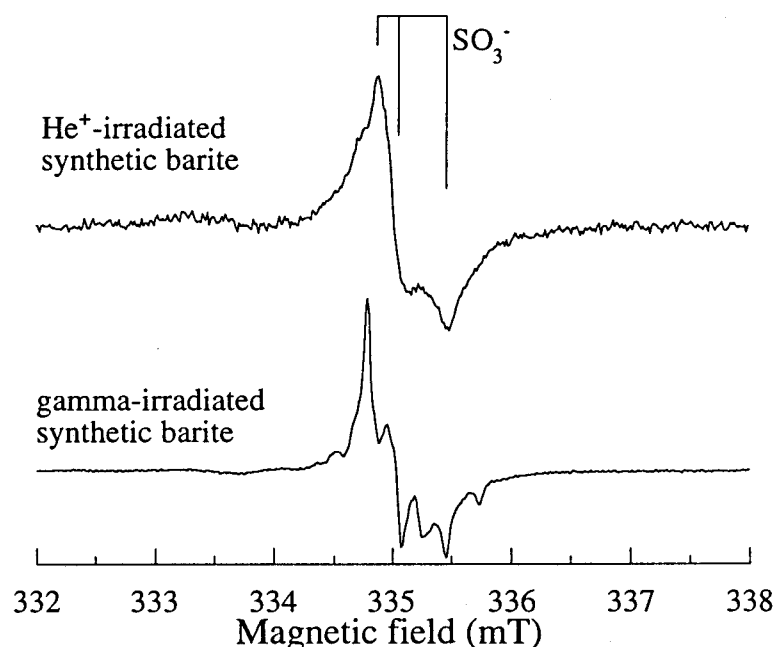

Fig. 4-12: The cw-ESR spectra of He$^+$-irradiated and gamma-irradiated synthetic barite measured at room temperature. The signal of the orthorhombic SO$_3^-$ was observed in both spectra, while no hole-type center was detected.

ESE spectrum of gamma-irradiated barite rose shows only the signal of SO$_3^-$ (Fig. 4-13). The phase relaxation time of the hole-type center may be so short that it cannot be observed at room temperature. The decay of ESE of SO$_3^-$

gives a phase relaxation time of 3.00 ± 0.05 μs at room temperature. A contribution of the instantaneous diffusion seems to be negligible since the phase relaxation time does not depend on the pulse width. The phase relaxation time may be governed by a spectral diffusion process.

Pulsed ESR and cw-ESR measurements at 77 K were performed for the barite rose. The cw-ESR spectrum and the field sweep ESE spectrum are shown in Fig. 4-14, where the signals of both hole-type center and SO_3^- ($T_2 = 2.38 \pm 0.02$ μs) were observed in the ESE spectrum. The signal of SO_3^- was already saturated and was not enhanced by additive gamma-irradiation, while that of hole-type centers grew as shown in Fig. 4-15 giving the total dose of 1.03 ± 0.37 kGy.
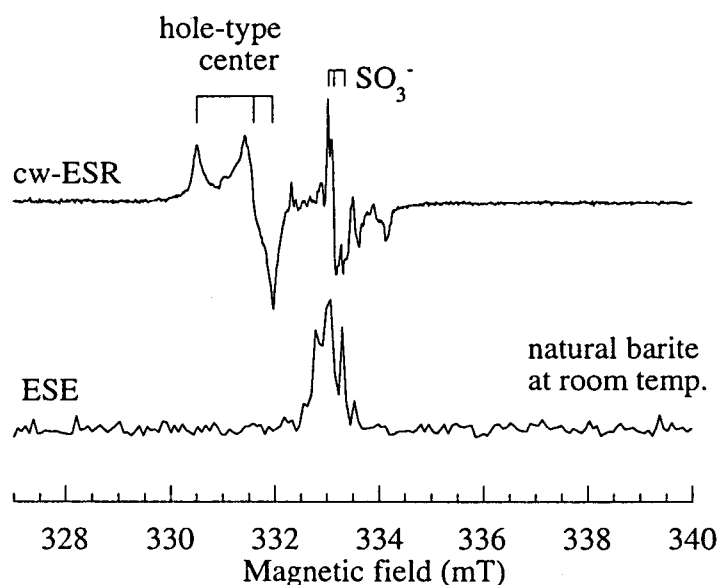

Fig. 4-13: The cw-ESR and ESE spectra of gamma-irradiated barite rose from the United States measured at room temperature, where the interpulse time was 400 ns. Hole-type center is clearly observed in cw-ESR spectrum. Only the echo due to SO_3^- was detected. The decay of the echo gives a phase relaxation time of 3.00 ± 0.05 μs.

hole-type center

cw-ESR

SO₃⁻

ESE

natural barite
at 77 K

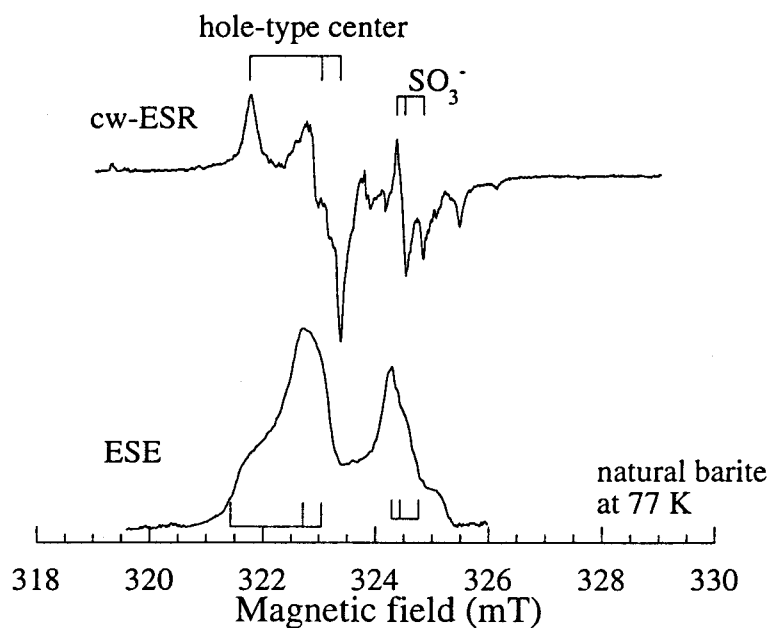318   320   322   324   326   328   330
Magnetic field (mT)

Fig. 4-14: The cw-ESR spectrum and the field sweep ESE spectrum of the gamma-irradiated barite rose measured at 77 K. The interpulse time was 500 ns. The obtained phase relaxation time of SO_3^- was 2.38 ± 0.02 μs. The hole-type center was also observed.
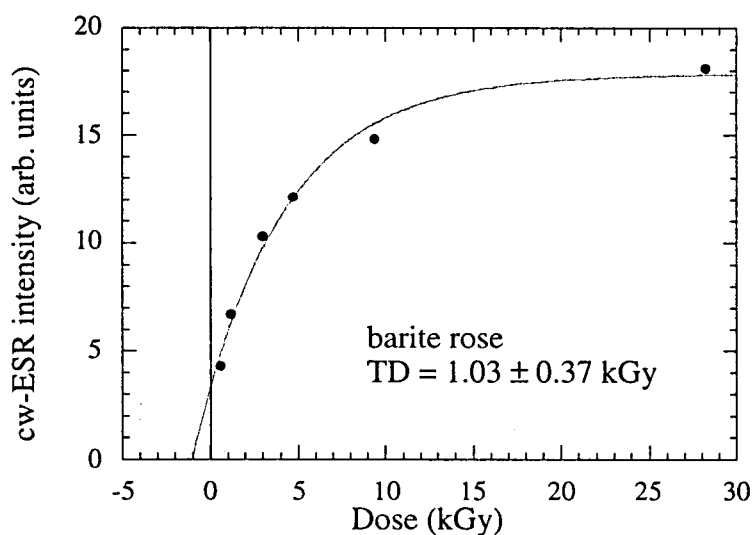
barite rose
TD = 1.03 ± 0.37 kGy

Fig. 4-15: The growth curve of hole-type center in the barite rose. The total dose of 1.03 ± 0.37 Gy was obtained.

Figure 4-16 shows the linear correlation between cw-ESR intensity of hole-type center measured at room temperature and the reciprocal of the phase relaxation time, T_2 , measured at 77 K. The observed relaxation time ranges from 1.91 to 3.08 µs because of the spin-spin interaction of the hole-type centers.

The concentration of spins, C, is described as

$$\frac{1}{T_2} = b_0 + \alpha C . \tag{4-3}$$

Fitting of data to eq. (4-3) gives b_0 of 0.2688 MHz which corresponds to a relaxation time of 3.72 µs. The concentration of spins is expressed as follows,

$$C = C_\infty \left\{ 1 - \exp\left(-a(d + D_t)\right) \right\} , \tag{4-4}$$

where d is dose, D_t is total dose and a is production efficiency. We obtain following expression,

$$\frac{1}{T_2} = b_0 + p\left\{ 1 - \exp\left(-a(d + D_t)\right) \right\}$$

$$= (b_0 + p)\left\{ 1 - \frac{ph}{b_0 + p}\exp(-ad) \right\} \tag{4-5}$$

$$\because h = \exp(-aD_t)$$

Figure 4-17 shows the fitting of data to the eq. (4-5) and the total dose of 1.4 kGy was obtained using b_0 = 0.2688 MHz. Total dose can be determined by the phase relaxation time using ESE method if b_0 is constant for the material.
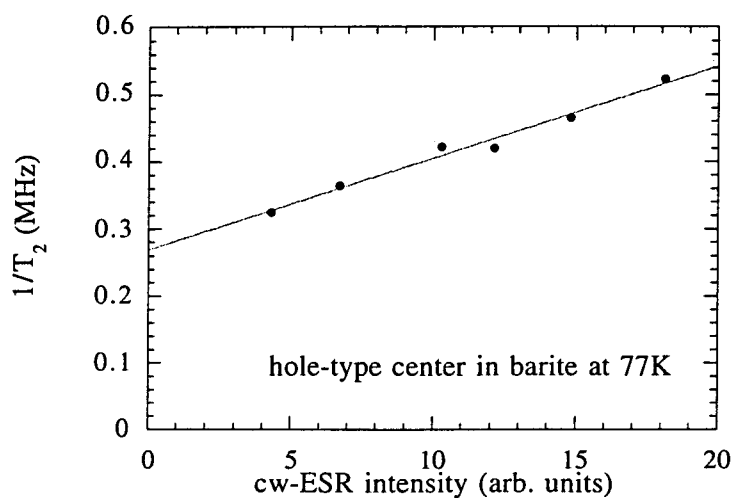
Fig. 4-16: The correlation between cw-ESR intensity of hole-type center measured at room temperature and the reciprocal of the phase relaxation time, T_2 measured at 77 K. The intercept of the vertical-axis fives the relaxation time of 3.72 μs which means the relaxation time when the concentration of spin is zero.
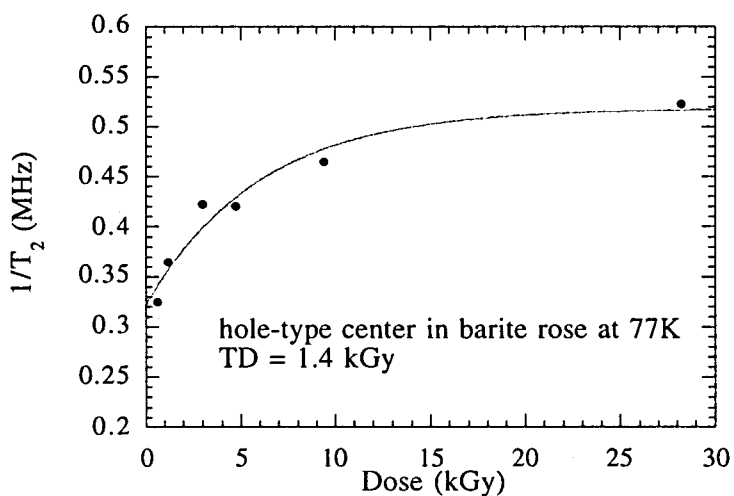

Fig. 4-17: The reciprocal of T_2 plotted as a function of the additive gamma dose.

Conclusions

Radiation induced defects in $CaCO_3$, SiO_2, $NaHCO_3$, $CaSO_4 \cdot 2H_2O$ and $BaSO_4$ were investigated using both cw-ESR and pulsed ESR. A new method of electron spin echo (ESE) dating and dosimetry was proposed. Conclusions of the present study are as follows.

1. Defects induced by alpha- (He^+ beam) irradiation were compared with those by gamma-irradiation for $CaCO_3$ (both aragonite and calcite). Characteristics of CO_2^- radicals in $CaCO_3$ were determined from the view points of linewidth, microwave power dependence and electron spin echo measurements.

2. Pulsed ESR provided the spin-spin relaxation times, $T_2 = 1.25 \pm 0.04$ μs for orthorhombic CO_2^- in gamma-irradiated modern coral and $T_2 = 1.58 \pm 0.02$ μs in nonirradiated fossil shell. The signal of the isotropic CO_2^- is found to be almost removed in the field sweep electron spin echo (ESE) spectrum, and the selective detection of orthorhombic CO_2^- becomes possible. Intensity of ESE is enhanced by the additive gamma-irradiation leading to the equivalent dose of 940 ± 720 Gy.

3. Intense signals of Mn^{2+} in the cw-ESR spectrum of a calcitic shell were removed in a field sweep ESE spectrum suggesting the usefulness of ESE in geological and archaeological dating where intense ESR signals associated with paramagnetic impurities such as Mn^{2+} in natural samples interfere the signal of defects produced by natural radiation beyond detection.

4. E' centers in quartz irradiated by alpha-rays (He^+-beam), neutrons, and those produced by gamma-irradiation after crushing as well as in gamma-irradiated silica glass were investigated. Line-shape of E' centers produced by alpha-rays was similar to those by neutrons but different from those gamma-rayed in silica glass. E' centers in crushed quartz were localized in

71

amorphous region presumably around micro cracks. The obtained phase relaxation times, T_2, are 6.5 ± 0.4 μs (by alpha-rays), 15.9 ± 1.0 μs (by neutrons), 7.3 ± 0.2 μs (by crushing and gamma-rays) and 18.5 ± 0.2 μs (in glass) and were compared with the line-widths and the ratios of homogeneous to inhomogeneous broadening obtained from the microwave power dependency.

5. Rokko fault, Japan was dated to be 69 ± 14 ka and 1.4 ± 0.5 Ma by signal separation technique using the difference of the shape of ESR signals. The ESR signal intensity of "amorphous-type" component of E' center was enhanced by additive gamma-irradiation, while that of "crystal-type" component was not.

6. Molecular species of HCO_3 and HCO_2, $(HCO_3)_2^-$ and HCO_2 were observed in synthetic $NaHCO_3$ (nahcolite) by gamma- and He^+-irradiation, respectively. Selective detection of HCO_2 in gamma-irradiated nahcolite was performed with pulsed ESR. Electron spin echo envelope modulation (ESEEM) due to presumably neighboring Na nuclei was observed on the spin echo decay curve of HCO_2 signal. An alpha effectiveness in producing defects, k-value, of 0.11 was obtained. Natural nahcolite collected from Searles Lake, California was dated to be 9.4 ± 8.8 Ma.

7. Defects produced by alpha (He^+ beam) and gamma irradiation in gypsum and barite were studied. SO_3^- at $g = 2.004$ in gamma-irradiated synthetic gypsum was selectively detected using electron spin echo. The phase relaxation time of hole-type centers ($g = 2.019$, 2.013 and 2.01) in barite desert rose irradiated (28.2 kGy ~ 0.597 kGy) at room temperature ranges from 1.91 μs to 3.08 μs at 77 K giving a total dose of 1.4 kGy.

Acknowledgments

First of all, I wish to express my sincere gratitude to my promoter, Professor Motoji Ikeya (Osaka University) for giving me advice, encouragement and, most of all, a positive mental attitude.

I am grateful to Associate Professor Itsuo Katakuse and Mr. Toshio Ichihara (Osaka Univ.) for their diligent cooperation and invaluable discussions in experiments. I am also grateful to Dr. Chihiro Yamanaka (Osaka Univ.), Dr. Shin Toyoda (McMaster University, Canada), Dr. Sumiko Ikeda (Tokyo Metropolitan University), Dr. Ayako Kai (Yamaguchi Univ.), Dr. Tatsuro Fukuchi (Yamaguchi Univ.), Dr. Masahiro Furusawa (Japan Advanced Institute of Science and Technology), Prof. Toshikatu Miki (Yamaguchi Univ.) for encouraging discussions and advice. I acknowledge my colleague, Mr. Hideki Sasaoka, Mr. Makoto Hirai, Mr. Atsushi Tani, Mr. Kazutoshi Ogoh and other all members of Ikeya laboratory.

I acknowledge my new promoter, Professor Mitsuji Hirata and Associate Professor Seiji Takeda for their encouragement of this thesis.

The gamma-irradiations and first-neutron-irradiation were made at the Institute of Scientific and Industrial Research and Department of Nuclear Engineering, Osaka University, and X-ray diffraction measurements were made at Ohtaka laboratory, Osaka University. I acknowledge Dr. Yuji Horino (Osaka National Research Institute, AIST) for He^+-irradiation.

For permission to reproduce figures and tables, I am indebted to Prof. M. Ikeya, Dr. A. Kai, Dr. S. Toyoda, Dr. J. A. Weil, Dr J. K. Rudra, Dr. W. B. Fowler, Dr. R. L. Sass, Dr. R. F. Scheuerman, Dr. W. A. Deer and the following publishers; World Scientific, Academic Press Ltd., Longman Group UK, American Physical Society and MUNKSGAARD International Booksellers and Publishers Ltd.

References

Albuquerque Antonio R. P. L. and Isotani, S. (1982): The EPR spectra of X-ray irradiated gypsum. *J. Phys. Soc. Jpn.* **51**, 1111-1118.

Bershov L. V., Martirosyan V. O., Marfunin A. S. and Speranski A. V. (1971): The yttrium-stabilized electron-hole centers in anhydrite. *Phys. Status Solid* (b)**44**, 505.

Callens, F., Debuyst, R., Dejehet, F., Idrissi, S. and Moens, P. (1994): Location and motion of isotropic paramagnetic centres in synthetic monohydrocalcite. *Jpn. J. Appl. Phys.* **33**, 4044-4050.

Caniére, P. De, Debuyst, R. Dejehet, F. and Appers, D. (1982): ESR study of radiation effects in ^{210}Po doped calcium carbonate: contribution to the estimation of the paleodose in a stalagmitic floor. *Radiochem. Radioanal. Lett.* **50**, 345-353.

Caniére, P. De, Debuyst, R. Dejehet, F. and Appers, D. (1986): ESR dating: A study of ^{210}Po-coated geological and synthetic samples. *Nucl. Tracks Radiat. Meas.* **11**, 211-220.

Caniére, P. De, Debuyst, P., Dejehet, F. and Appers, D. (1988): ESR study of internally a-irradiated (^{210}Po nitrate doped) calcite single crystal. *Nucl. Tracks Radiat. Meas.* **14**, 267-273.

Castner, T. G. (1959): Saturation of the paramagnetic resonance of a V center. *Phys. Rev.* **115**, 1506-1515.

Debuyst, R., Caniére, P. De. and Dejehet, F. (1990): Axial CO_2^- in α-particle irradiated calcite: potential use in ESR dating. *Nucl. Tracks. Radiat. Meas..* **17**, 525-530.

Debuyst, R., Bidiamambu, M and Dejehet, F. (1991): An ESR study of γ - and α-irradiated synthetic powdered calcite labelled with ^{13}C. *Nucl. Tracks. Radiat. Meas.* **18**, 193-201.

Deer, W. A., Howie R. A. and Zussman, J. (1966): *An introduction to Rock forming minerals* (Longman, Essex)

Dikanov, S. A. (1981): Modulation effects in the electron spin echo resulting from hyperfine interaction with a nucleus of an arbitrary spin. *J. Magn.*

Reson. **42**, 474-487.

Garrison, E. G., Rowlett, R. M., Cowan, D. L. and Holroyd, L.V. (1981): ESR dating of ancient flints. *Nature* **290**, 44-45.

Griscom, D. L. (1979): E' center in glassy SiO_2: microwave saturation properties and confirmation of the primary [29]Si hyperfine structure. *Phys. Rev. B* **20**, 1823-1834.

Grün, R. and Schwarcz, H. P. (1988): Electron spin resonance dating of the pleistocene coral reef tracts of Barbados. *Quaternary Research* **29**, 197-215.

Holmberg, R. W. (1971): ESR study of γ-irradiated single crystal of potassium bicarbonate at 77 K. *J. Chem. Phys.* **55**, 1730-1735.

Ikeda, S. and Ikeya, M. (1992): ESR signals in natural and synthetic gypsum: an application of ESR to the age estimation of gypsum precipitates from San Andreas Fault. *Jpn. J. Appl. Phys.* **31**, L136-L138.

Ikeya, M. and Kai, A. (1988): ESR dating of saline sediments using $NaHCO_3$ and NaCl. *Quatern. Sci. Rev.* **7**, 471-475.

Ikeya, M., Kohno, H., Toyoda, S. and Mizuta, Y. (1992): Spin-spin relaxation time of E' centers in Neutron-irradiated quartz (SiO_2) and in fault gouge. *Jpn. J. Appl. Phys.* **31**, L1539-L1541.

Ikeya, M. (1993): *New application of electron spin resonance: dating, dosimetry and microscopy*, World Scientific, Singapore.

Jani, M. G., Bossoli, R. B. and Halliburton, L. E. (1983) Further characterization of the E_1' center in crystalline SiO_2. *Phys. Rev. B* **27**, 2285.

Kai, A. (1992): *Effects of impurities on radiation-induced radicals in $CaCO_3$ and its application to ESR dating and dosimetry* (Ph. D thesis)

Kai, A. and Miki, T. (1992): Electron spin resonance of sulfite radicals in irradiated calcite and aragonite. *Radiat. Phys. Chem.* **40**, 311-314.

Kasuya, M., Brumby, S. and Chappell, J. (1991a) ESR signals from natural gypsum single crystals: implications for ESR dating. *Nucl. Tracks Radiat. Meas.* **18**, 329.

Kasuya, M., Kato, M. and Ikeya, M. (1991b) ESR signals of natural barite ($BaSO_4$) crystals: possible application to geochronology. *Essats in Geology, Plof. H. Nakagawa Commemorative Volume* 95-98.

Katzenberger, O., Debuyst, R., Canniére, P. De, Dejehet, F., Appers, D. and Barabas, M. (1989): Temperature experiments on mollusc sample: an

approach to ESR signal identification. *Appl. Radiat. Isot.* **40**, 1113-1118.

Lyons, R. G., Wood, W. B. and Williams, P. W. (1985): Determination of alpha efficiency in speleothem calcite by nuclear accelerator techniques. ESR Dating and Dosimetry (Ionics, Tokyo) 39-48.

Lyons, R. G. (1988): Determination of alpha effectiveness in ESR dating using nuclear accelerator techniques: methods and energy dependence. *Nucl. Tracks Radiat. Meas.* **14**, 275-280.

Lyons, R. G. and Brennan, B. J. (1989): Alpha-particle effectiveness in ESR dating: energy dependence and implications for dose-rate calculations. *Appl. Radiat. Isot.* **40**, 1063-1070.

Lyons, R. G. and Brennan, B. J. (1991): Alpha/gamma effectiveness ratios of calcite speleothems. *Nucl. Tracks Radiat. Meas.* **18**, 223-227.

Marshall, S. A., Reinberg, A. R., Serway, R. S. and Hodges, J. A. (1964): Electron spin resonance absorption spectrum of CO_2^- molecule-ions in single crystal calcite. *Molec. Phys.* **8**, 225-231.

Miki, T. and Kai, A. (1990): Rotating CO_2^- centers in corals and related materials. *Jpn. J. Appl. Phys.* **29**, 2191-2192.

Nuttall, R. H. D. and Weil, J. A. (1981): The magnetic properties of the oxygen-hole aluminum centers in crystalline SiO_2, I. [AlO_4]. *Can. J. Phys.* **59**, 1696-1708.

O'Brien M. C. M. (1955) The structure of the colour centers in smoky quartz. *Proc. Roy. Soc. A* **231**, 404.

Rink, W. J. and Odom, A. L. (1991): Natural alpha recoil particle radiation and ionizing radiation sensitivities in quartz detected with ESR: implications for geochronometry. *Nucl. Tracks Radiat. Meas.* **18**, 163-173.

Rowan, L. G. Hahn, E. L. and Mims, W. B. (1965): Electron-spin-echo envelope modulation. *Phys. Rev. A* **137**, 61-71.

Rudra, J. K. and Fowler, W. B. (1987) Oxygen vacancy and E'_1 center in crystalline SiO_2. *Phys. Rev. B* **35**, 8223.

Ryabov, I. D., Bershov, L. V. and Ganeev, I. G. (1983) Electron paramagnetic resonance of PO_3^{2-} and SO_3^- radicals in barite. *Phys. Chem. Minerals* **10**, 21-26.

Sass, R. L. and Scheuerman, R. F. (1962): The crystal structure of sodium bicarbonate. *Acta Cryst.* **15**, 77-81.

Toyoda, S. (1992): *Production and decay characteristics of paramagnetic defects in quartz: applications to ESR dating* (Ph. D thesis)

Toyoda, S., Kohno, H. and Ikeya, M. (1993): Distorted E'_1 centers in crystalline quartz; an application to ESR dating of fault movements. *Appl. Radiat. Isot.* **44**, 215-220.

Weil, J. A. (1984) A review of electron spin spectroscopy and its applications to the study of paramagnetic defects in crystalline quartz. *Phys. Chem. Minerals* **10**, 149.

Wieser, A. and Regulla, D. F. (1989): ESR dosimetry in the "Giga-rad" range. *Appl. Radia. Isot.* **40**, 901-913.

Wintle, A. G. (1978): A thermoluminescence dating study of some Quaternary calcite: potential and problems. *Can. J. Earth Sci.* **15**, 1977-1986.

Wray, J. L. and Daniels, F. (1957): Precipitation of calcite and aragonite. *J. Am. Chem. Soc.* **79**, 2031-2034.

List of publications and presentations

Publications

1. Toyoda, S. Kohno, H. and Ikeya, M.
    E_1' centers in distorted sites in quartz: ESR dating of geological fault.
    Adv. ESR Appl., vol. 7, pp. 2-4, (1991)

2. Ikeya, M., Kohno, H., Toyoda, S. and Mizuta, Y.
    Spin-spin relaxation time of E' centers in neutron-irradiated quartz (SiO_2) and in fault gouge.
    Jpn. J. Appl. Phys., vol. 31, (1992) pp. L1539-L1541, Part 2, No. 11A

3. Toyoda, S., Kohno, H., and Ikeya, M.
    Distorted E_1' centers in crystalline quartz: an application to ESR dating of fault movements.
    Appl. Radiat. Isot., vol. 44, No. 1/2, pp. 215-220, (1993)

4. Kohno, H. , Yamanaka, C. , Ikeya, M., Ikeda, S. and Horino, Y.
    An ESR study of radicals in $CaCO_3$ produced by 1.6 MeV He^+-and γ-irradiation.
    Nucl. Inst. Method Phys. Res. B 91 (1994) 366-369.

5. Kohno, H. , Yamanaka, C. and Ikeya, M
    Pulsed and cw-ESR studies of CO_2^- in $CaCO_3$ irradiated by He^+ and γ rays for ESR dating.
    Jpn. J. Appl. Phys., vol. 33 No. 10, Part 1, (1994) 5743-5746.

6. Kohno, H. , Yamanaka, C. , Ikeya, M and Y. Horino
    Pulsed and cw-ESR Study of E' and Al Hole Centers in Quartz Produced by Irradiations and Crushing.
    Appl. Magn. Reson. vol. 9/4 pp. 481-489 (1995)

7. Kohno, H. and Yamanaka, C.
    Amplitude Modulation Electron Spin Resonance for Signal Separation Using the Difference of Microwave Power Dependence.
    Adv. ESR Appl. **11** (1996) 10-16.

8. Kohno, H., Yamanaka, C. and Ikeya, M.
    Effects of Alpha-Irradiation and Pulsed ESR Measurements of Evaporites.
    Appl. Radiat. Isotop. **47** (1996) 1459-1463.

9. Tani, A., Kohno, H., Yamanaka, C. and Ikeya, M.
   ESR Dating of Geological Fault with a New Isochrone Method, Granite
   Fractured on the Earthquake in 1995.
   Appl. Radiat. Isotop. **47** (1996) 1423-1426.
10. Yamanaka, C., Kohno, H. and Ikeya, M.
    Pulsed ESR measurements of oxygen deficient type centers in various
    quartz.
    Appl. Radiat. Isotop. **47** (1996) 1573-1577.

Japanese article
1. 河野日出夫・小村哲司・池谷元伺
   ESR年代測定と古環境の解明
   アイオニクス No. 220, pp. 27-31, (1994)
2. 成瀬敏郎・柳精司・河野日出夫・池谷元伺
   電子スピン共鳴（ESR）による中国・韓国・日本の風成塵起源石英
   の同定
   第四紀研究 (The Quaternary Research) 35 (1996) 25-34.

Presentations (international symposium)
1. H. Kohno, C. Yamanaka, M. Ikeya, S. Ikeda and Y. Horino
   An ESR Study of Radicals in $CaCO_3$ produced by 1.6 MeV He^+- and
   γ-irradiation
   Radiation Effects in Insulators-7, Nagoya Univ., Sep. 1993
2. H. Kohno and M. Ikeya
   Electron spin resonance (ESR) dating of evaporites
   International symposium and workshop on paleoenvironmental records of
   desert margins and paleomonsoon variation during the last 20ka, Xi'an,
   Aug. 1994
3. H. Kohno, C. Yamanaka and M. Ikeya
   Effects of Alpha-Irradiation and Pulsed ESR Measurements of Evaporites
   4th International Symposium on ESR Dosimetry and Applications, München,
   May. 1995

APPENDIX

Microwave Power Amplitude Modulation Electron Spin Resonance (AM-ESR): First Derivative Microwave Power Dependence

Abstract

The first derivative curves of the microwave power dependence of the signal intensity in electron spin resonance (ESR) measurements were obtained using double modulation of the microwave power modulation at 6 Hz and the magnetic field modulation at 100 kHz. A spectrometer was specifically made using a PIN diode and home-made microwave bridge. The signals of CO_2^- in hydroxyapatite and E' centers in quartz have been measured to study the saturation behavior of the signal intensity against applied microwave power.

§1 Introduction

An ordinary spectrometer of electron spin resonance (ESR) employes 100 kHz magnetic field modulation and detects the first-derivative signal by amplifying using lock-in amplifier. Clerjaud and Lambert, 1971 reported a high sensitivity ESR spectrometer using microwave modulation, where the reflected microwave power from cavity was modulated by a PIN diode.[1] They applied the microwave modulation at 100 kHz and magnetic field modulation at low-frequency (80 Hz) to make experiments at low temperature with a high sensitivity.

A microwave-power dependence of ESR signal intensity has been used for the characterization of the signal. No technique was available to obtain a first derivative curve of the microwave power dependence of the signal intensity in spite of its sensitivity to the change in the shape of the curve. A PIN diode used

on our spectrometer modulates the microwave power which incidents into the cavity but not the reflected microwave power from the cavity. Our modulation method allows the measurement of the first derivative microwave power dependence. One can remove a signal or obtain an inverse signal by adjusting the applied microwave power.

§2 Experimentals

(a)   Apparatus for microwave power modulation

The schematic diagram of the microwave bridge is shown in Fig. 1. The microwave power produced by a Gunn diode is modulated by a PIN diode and reaches to the cavity. The reflected microwave which bypasses is not affected by the PIN modulator. The microwave modulation frequency was set to 6 Hz in this experiment and the modulation amplitude was controlled by a voltage-control PIN driver and a function generator. The DC bias of +0.2 V and the modulated bias of 0.1 V were applied to the PIN diode with the power attenuation of 10 dB/V. The incident microwave power into the cavity is expressed as

$$\log_{10}P_1 = \log_{10}P_2 - 0.1 \cdot \{2+\sin(2\pi ft)\} \ ,$$

where P_1 is the microwave power applied to a sample, P_2 is the initial power in mW, f is the modulation frequency and t is the time.

The homemade microwave bridge was adopted to a commercial X-band ESR spectrometer (JEOL, RE-1X). The magnetic field modulation amplitude was 0.1 mT at a frequency of 100 kHz. The output from Ga-As detector was amplified by 100 kHz lock-in amplifier and then by 6 Hz lock-in amplifier. All the measurements were performed at room temperature.
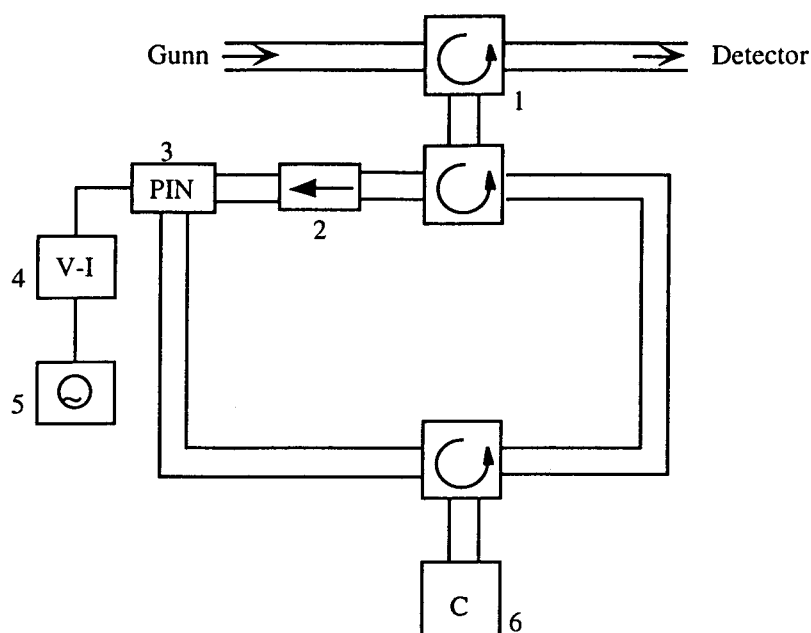
Fig. 1: Block diagram of the microwave bridge: 1, circulator; 2, isolator; 3, PIN modulator; 4, PIN driver; 5, function generator; 6, cavity.

(b) Samples

A fossil tooth of a shark was crushed into powder and used for ESR measurement. Following three quartz samples were also measured:

Sample C: crushed quartz with the fractions under 5 μm in diameter and gamma-irradiated to the dose of 435 Gy.

Sample F: geological fault gouge collected from Rokko fault, Japan.

Sample N: quartz irradiated by 14-MeV fast neutrons to a dose of 2.4×10^{14} n/cm^2 using an Oktavian accelerator utilizing the D-T reaction by the bombardment of D$^+$ on a titanium-tritium target.

§3 Principle of ESR power modulation spectroscopy

Figure 2 shows the principle of the microwave modulation method. ESR absorption increases in proportion to the square root of the microwave power at a low microwave power (the stage-I). The intensity reaches to the maximum

(the stage-II) and will decreases (the stage-III) if the inhomogeneous line broadening is not so dominant.
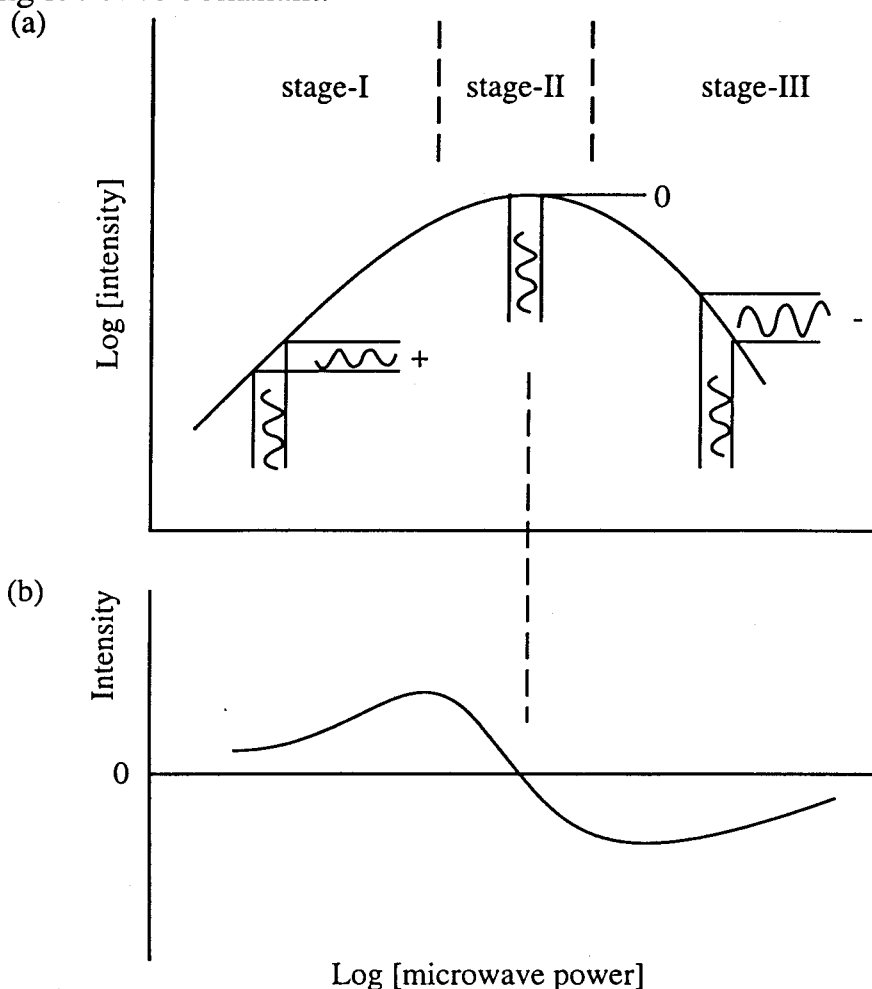

Fig. 2: Principle of the measurement of the first derivative microwave power dependence using the microwave modulation method: (a) ESR intensity plotted as a function of microwave power; (b) the intensity obtained by double modulation method. The intensity obtained by microwave power modulation method is zero at the top of the microwave power dependence curve using ordinary method and the phase of the ESR signal inverts at this point.

The amount of ESR absorption is modulated by the modulation of the applied microwave power. The modulation of ESR intensity at the stage-III has an inverse phase of that at the stage-I. At the maximum of ESR absorption (the stage-II), the output from the lock-in amplifier is zero because no modulation of

the same frequency is caused. However, the second-harmonic modulation is expected at the local maximum. The first derivative curve of the microwave power dependence of ESR intensity can be obtained by this method as expressed as

$$g(\log_{10}P) = df(\log_{10}P)/d[\log_{10}P] ,$$

where $f(\log_{10}P)$ is a curve of the microwave power dependence of ESR intensity and $g(\log_{10}P)$ is a first derivative curve obtained by the modulation method.

§4 Results

(a) CO_2^- in hydroxyapatite

Figure 3 shows ESR spectra of a fossil tooth of shark (hydroxyapatite, $Ca(PO_4)_6(OH)_2$) measured using (a) the ordinary method and (b) the double modulation of the microwave power and the magnetic field, where the microwave power was 6 mW before the PIN modulator and was attenuated for 2 dB by the DC bias of 0.2 V for both measurements. The orthorhombic CO_2^- radical with the g-factor of 2.0036, 2.0023 and 1.9975[2] is the main species and some additional signals were also detected for both measurements. Two spectra are very similar. It means that the saturation behavior of these signals are almost the same at this microwave power.
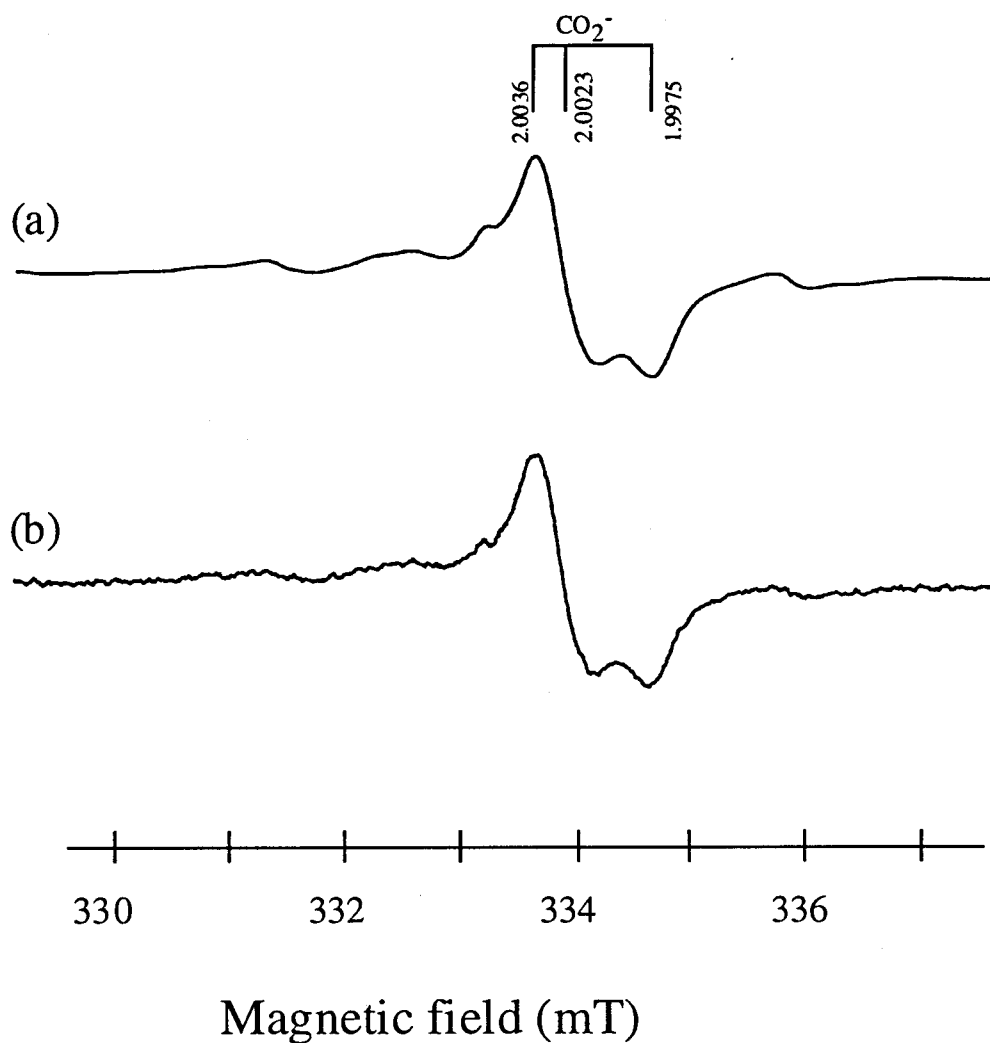
Fig. 3: ESR spectra of a fossil tooth of a shark measured using a) the ordinary method and b) the double modulation of the microwave power and the magnetic field, where the microwave power was 6 mW (the incident microwave power into the cavity was 3.8 mW) for both measurements.

The microwave power dependence of the signal of CO_2^- is shown in Fig. 4. ESR intensity obtained by the ordinary method saturates at the microwave power of about 100 mW. Inhomogeneous broadening may be a reason why the signal intensity does not decrease at a high microwave power. The microwave power dependence indicates that ESR intensity obtained by the double modulation

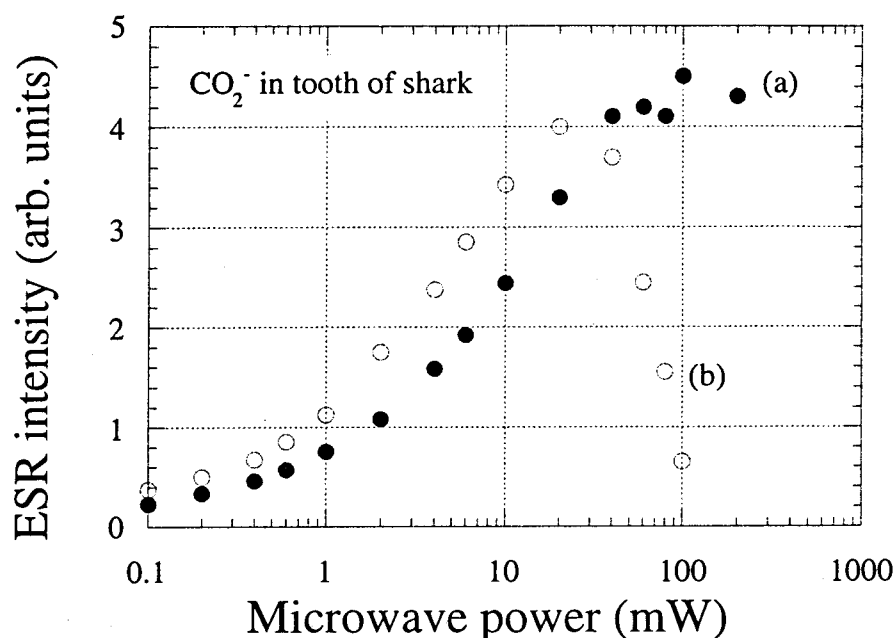method saturates at about 20 mW and decreases promptly to almost zero at 100 mW.

Fig. 4: The microwave power dependence of the signal of CO_2^- obtained using (a) the ordinary method and (b) the double modulation method.

(b) E' centers in quartz

The difference in the saturation behavior is an important information on the characterization of a signal. It is expected that the derivative curve gives the additional information. The ESR signal of a lattice defect, E' center[3] (an unpaired electron at an oxygen vacancy with the g-factors of 2.0003, 2.0005 and 2.0018) in quartz was measured by the microwave modulation technique. The shape of the ESR signal of E' centers in crushed and gamma-irradiated quartz is similar to that in amorphous SiO_2 while that in neutron-irradiated quartz is "crystal-type" [4]. It is expected that a part of E' centers in quartz in fault gouge is the "crystal-type" and another part is the "amorphous-type". The ESR signal must be a linear combination of these two spectra.
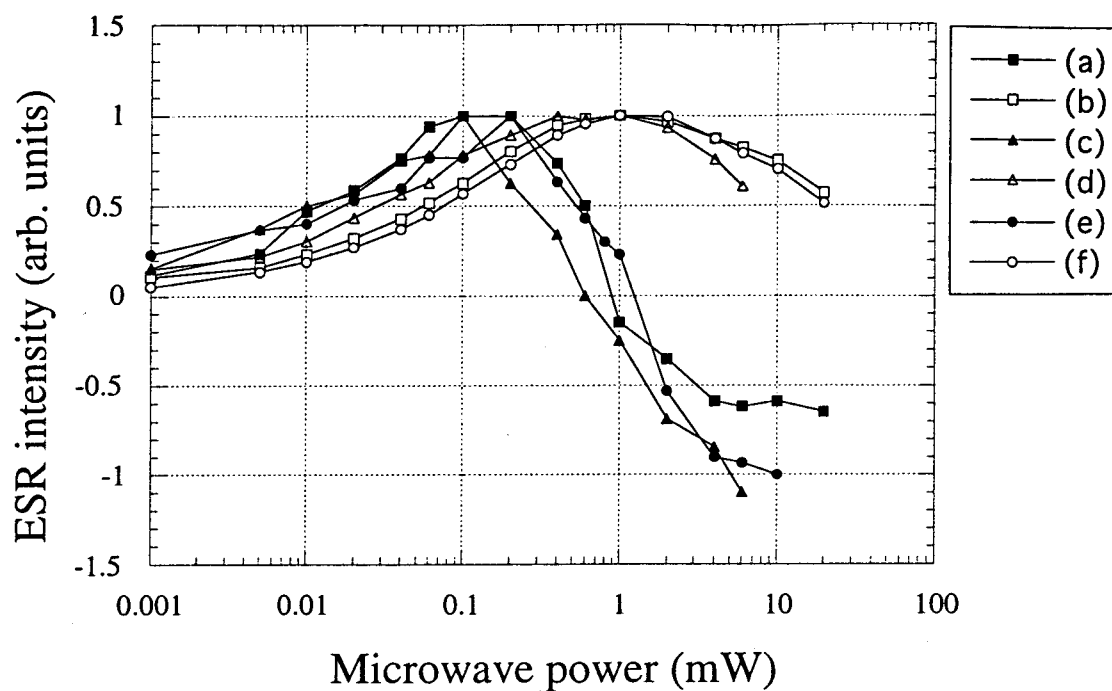
Fig. 5: The microwave power dependence of the ESR signal intensity of E' center in [(a) and (b)] crushed and gamma-irradiated quartz, [(c) and (d)] neutron-irradiated quartz and [(e) and (f)] geological fault gouge. Open and close symbols represent the ordinary measurements and the double modulation measurements, respectively.
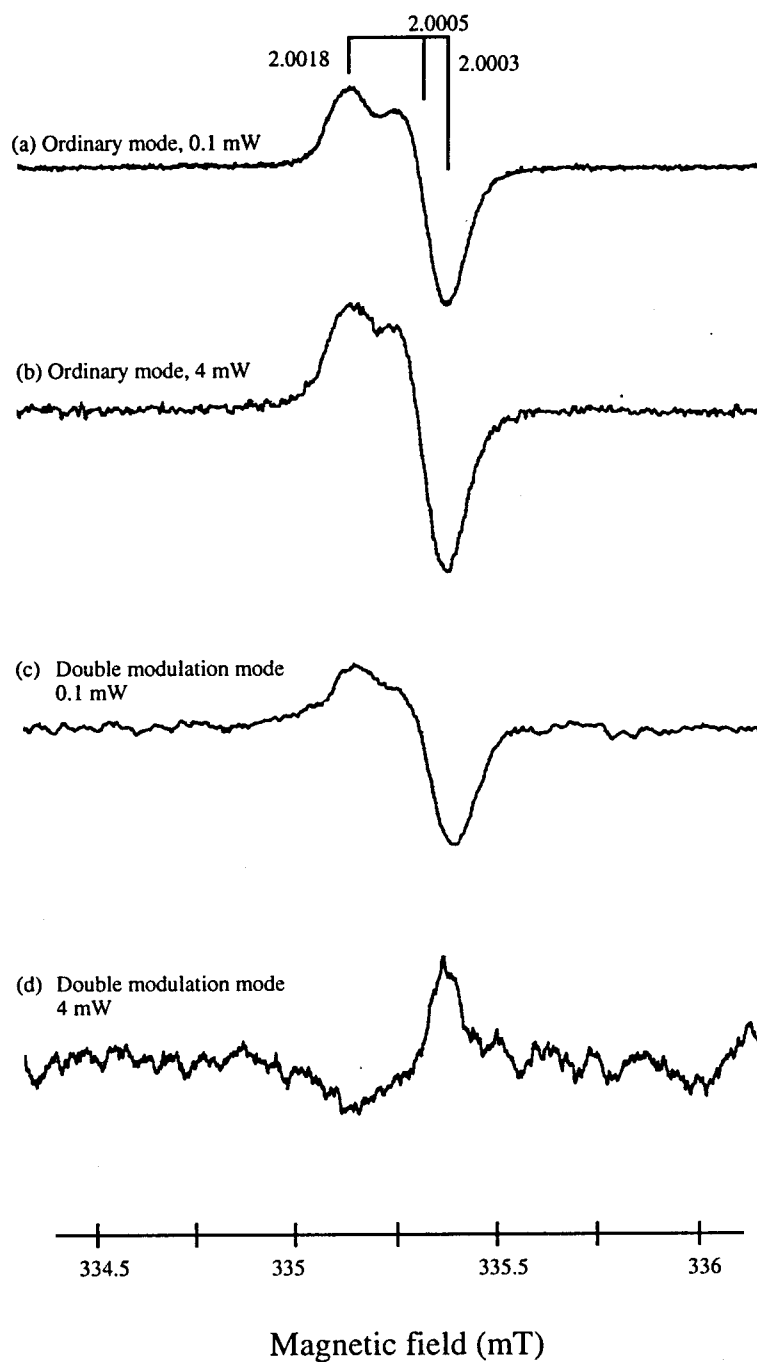
Fig. 6: ESR spectra of E' centers in the crushed and gamma-irradiated quartz: (a) the ordinary mode, 0.1 mW; (b) the ordinary mode, 4 mW; (c) the double modulation mode, 0.1 mW; (d) the double modulation mode, 4 mW.

The microwave power dependence of the intensity of E' centers is shown in

Fig. 5 for Sample C, N and F. ESR spectra of E' centers in the crushed and gamma-irradiated quartz measured at the microwave power of 0.1 mW and 4 mW (before PIN diode) are shown in Fig. 6. The signal intensities obtained by normal mode saturate at about 1 mW and constantly decrease for all the sample. Correspondingly, the negative intensity was obtained using the double modulation mode. The double modulation mode gives an inverted signal. The S/N for the double modulation detection was about 4 with a time constant of 10 s at 4 mW, while that for the ordinary method was 16 with a time constant of 0.3 s at 4 mW. It is one order of the magnitude worse for our home-made apparatus at the moment.

At the normal mode, the signal intensity of E' center in the Sample F behaves similar to that in the Sample C. The existence of the component of the "crystal-type" E' center cannot be confirmed by the saturation behavior obtained by the normal mode. The intensity of E' center in the sample-F obtained by the double modulation mode is also similar to that in the sample-C up to about 6 mW but decreases to the level of the Sample N at a high microwave power. Generally, the derivative curve is more sensitive to the change of the shape of the original curve. It is emphasized that the double modulation mode has enabled to distinguish the slight difference in the microwave power dependence. Signals with a similar spectrum but with a different relaxation time thus can be resolved with cw-ESR.

§5 Conclusion

The microwave power modulation detection of ESR has been used in the measurements for the signal of CO_2^- in hydroxyapatite and E' centers in quartz. The first derivative of the microwave power dependence of the signal intensity has been obtained using this method. This technique provides a selectivity on the signal detection and will be useful for ESR dating where signals with different relaxation times overlap[5]. A problem on ESR dating is that some overlapping signals interfere the measurement of the dating signal. The measurement using the microwave power modulation can remove a signal if it has a maximum intensity.

References

1) B. Clerjaud and B. Lambert, J. Phys. E, **4** (1971) 619.

2) H. Ishii and M. Ikeya, Appl. Radiat. Isotop. **44** (1993) 95.

3) M. G. Jani, R. B. Bossoli and L. E. Halliburton (1983) Phys. Rev. B **27** (1983) 2285.

4) H. Kohno, C. Yamanaka, M. Ikeya and Y. Horino, Appl. Magn. Reson. (in press).

5) M. Ikeya, *NEW APPLICATION OF ELECTRON SPIN RESONANCE: Dating, Dosimetry and Microscopy.* (World Scientific, Singapore, 1993)